NORSAR

ROYAL NORWEGIAN COUNCIL FOR SCIENTIFIC AND INDUSTRIAL RESEARCH

Scientific Report No. 1-81/82

SEMIANNUAL TECHNICAL SUMMARY

1 April 1981—30 September 1981

By
Jørgen Torstveit (ed.)

Kjeller, December 1981

SECURITY CLASSIFICATION OF THIS PAGE *(When Data Entered)*

REPORT DOCUMENTATION PAGE

READ INSTRUCTIONS BEFORE COMPLETING FORM

1. REPORT NUMBER: F08606-79-C-0001	2. GOVT ACCESSION NO.
3. RECIPIENT'S CATALOG NUMBER	
4. TITLE *(and Subtitle)*: SEMIANNUAL TECHNICAL SUMMARY 1 April - 30 September 1981	5. TYPE OF REPORT & PERIOD COVERED: 1 Apr - 30 Sep 1981
	6. PERFORMING ORG. REPORT NUMBER: Sci. Report 1/81-82
7. AUTHOR(s): J. Torstveit (ed.)	8. CONTRACT OR GRANT NUMBER(s)
9. PERFORMING ORGANIZATION NAME AND ADDRESS: NTNF/NORSAR, Post Box 51, N-2007 Kjeller, Norway	10. PROGRAM ELEMENT, PROJECT, TASK AREA & WORK UNIT NUMBERS: NORSAR Phase 3
11. CONTROLLING OFFICE NAME AND ADDRESS	12. REPORT DATE: Dec 1981
	13. NUMBER OF PAGES: 82
14. MONITORING AGENCY NAME & ADDRESS *(if different from Controlling Office)*: VELA Seismological Center, 312 Montgomery Street, Alexandria, VA 22314, USA	15. SECURITY CLASS. *(of this report)*
	15a. DECLASSIFICATION/DOWNGRADING SCHEDULE

16. DISTRIBUTION STATEMENT *(of this Report)*

APPROVED FOR PUBLIC RELEASE; DISTRIBUTION UNLIMITED.

17. DISTRIBUTION STATEMENT *(of the abstract entered in Block 20, if different from Report)*

APPROVED FOR PUBLIC RELEASE; DISTRIBUTION UNLIMITED.

18. SUPPLEMENTARY NOTES

19. KEY WORDS *(Continue on reverse side if necessary and identify by block number)*

20. ABSTRACT *(Continue on reverse side if necessary and identify by block number)*

This report describes the operation, maintenance and research activities at the Norwegian Seismic Array (NORSAR) for the period 1 April 1981 to 30 September 1981.

The performance of the NORSAR online detection processor system has decreased compared to the previous period; the DP uptime for this period is 89% The

DD FORM 1 JAN 73 1473 EDITION OF 1 NOV 65 IS OBSOLETE

SECURITY CLASSIFICATION OF THIS PAGE *(When Data Entered)*

Special Processing System (SPS) caused most of the downtime the first half of the period; in the last half period the main computer (360/40) caused most of the downtime.

A total of 1642 events were reported in this period, giving a daily average of 9 events. The number of reported events per month varies from 333 in April to 210 in July.

There have been some major breakdowns on some of the communications lines in this period, especially the NORESS system has been affected.

The most-used application programs are now converted to the new standards, or new programs have been developed. Data bases on disk both for instrument and bulletin data are being built up.

The research activity is briefly described in Section VI. The first subsection discusses constrained inversion for sources of finite extent. Subsection 2 is a work to devise an optimal sensor layout for a prototype regional seismic array. Subsection 3 describes an attempt to map seismically the deep structure beneath Iceland. Sections 4 and 5 deal with mantle heterogeneities beneath Fennoscandia and Eastern Europe. Section 6 describes a study on signal detection using P-wave envelope representation. Section 7 is an investigation of signal focusing effects at NORSAR for events near the Caspian Sea. Section 8 describes a three-dimensional ray-tracing system and the last section discusses a method (AR-method) for measurement of group velocities of seismic surface waves.

AFTAC Project Authorization No.	:	VELA VT/0702/B/PMP, Amendment 1
ARPA Order No.	:	2551
Program Code No.	:	0F10
Name of Contractor	:	Royal Norwegian Council for Scientific and Industrial Research
Effective Date of Contract	:	1 October 1979
Contract Expiration Date	:	30 September 1981
Project Manager	:	Frode Ringdal (02) 71 69 15
Title of Work	:	The Norwegian Seismic Array (NORSAR) Phase 3
Amount of Contract	:	$2.119.000
Contract Period Covered by the Report	:	1 April - 30 September 1981

This research was supported by the Advanced Research Projects Agency of the Department of Defense and was monitored by AFTAC, Patrick AFB FL 32925, under contract no.

NORSAR Contribution No. 310

TABLE OF CONTENTS

TABLE OF CONTENTS (cont.)

I. SUMMARY

This report describes the operation, maintenance and research activities at the Norwegian Seismic Array (NORSAR) for the period 1 April 1981 to 30 September 1981.

The performance of the NORSAR online detection processor system has decreased compared to the previous period; the DP uptime for this period is 89% The Special Processing System (SPS) caused most of the downtime the first half of the period; in the last half period the main computer (360/40) caused most of the downtime.

A total of 1642 events were reported in this period, giving a daily average of 9 events. The number of reported events per month varies from 333 in April to 210 in July.

There have been some major breakdowns on some of the communications lines in this period, especially the NORESS system has been affected.

The most-used application programs are now converted to the new standards, or new programs have been developed. Data bases on disk both for instrument and bulletin data are being built up.

The research activity is briefly described in Section VI. The first subsection discusses constrained inversion for sources of finite extent. Subsection 2 is a work to devise an optimal sensor layout for a prototype regional seismic array. Subsection 3 describes an attempt to map seismically the deep structure beneath Iceland. Sections 4 and 5 deal with mantle heterogeneities beneath Fennoscandia and Eastern Europe. Section 6 describes a study on signal detection using P-wave envelope representation. Section 7 is an investigation of signal focusing effects at NORSAR for events near the Caspian Sea. Section 8 describes a three-dimensional ray-tracing system and the last section discusses a method (AR-method) for measurement of group velocities of seismic surface waves.

II. OPERATION OF ALL SYSTEMS

II.1 Detection Processor (DP) Operation

There have been 191 breaks in the otherwise continuous operation of the NORSAR online system within the current 6-month reporting interval. The SPS has shown a remarkably good performance since the middle of July and has had just four stops in the last 2½ months. After a fire in the 360 computer used in DP online on 10 June, the other 360 computer is being used for DP processing. As can be seen from Table II.1.1 this computer is not as stable as the one used before. The uptime percentage for the period is 89.0 as compared to 91.2 for the previous period.

Fig. II.1.1 and the accompanying Table II.1.1 both show the daily DP downtime for the days between 1 April 1981 and 30 September 1981. The monthly recording times and percentages are given in Table II.1.2.

The breaks can be grouped as follows:

a)	SPS malfunction	123
b)	Error on the multiplexor channel	0
c)	Stops related to possible program errors	1
d)	Maintenance stops	9
e)	Power jumps and breaks	10
f)	Hardware problems	45
g)	Magnetic tape and disk drive problems	3
h)	Stops related to system operation	0
i)	TOD error stops	0

The total downtime for the period was 482 hours and 35 minutes. The mean-time-between-failures (MTBF) was 0.9 days as compared with 0.8 days for the previous period.

J. Torstveit

LIST OF BREAKS IN DP PROCESSING THE LAST HALF-YEAR

DAY	START		STOP		COMMENTS.....
93	16	52	19	5	SPS ERROR
93	19	34	22	1	SPS ERROR
95	11	47	12	0	SPS ERROR
96	20	28	21	25	SPS ERROR
97	3	41	5	43	SPS ERROR
99	2	38	6	9	SPS ERROR
99	23	29	24	0	SPS ERROR
100	0	0	0	10	SPS ERROR
100	18	38	20	0	SPS ERROR
100	20	21	21	7	SPS ERROR
101	19	1	19	51	SPS ERROR
103	12	54	13	29	SPS ERROR
103	23	0	24	0	SPS ERROR
104	0	0	0	2	SPS ERROR
104	9	5	9	34	SPS ERROR
104	15	35	18	42	SPS ERROR
105	2	55	6	21	SPS ERROR
105	11	16	11	30	SPS ERROR
106	16	0	17	35	SPS ERROR
106	18	51	19	43	SPS ERROR
106	20	6	23	17	SPS ERROR
110	1	44	2	25	SPS ERROR
111	14	34	16	30	SPS ERROR
112	0	18	1	14	SPS ERROR
112	5	8	9	38	SPS ERROR
113	10	19	10	28	SPS ERROR
115	16	30	17	15	SPS ERROR
115	23	22	24	0	SPS ERROR
116	0	0	0	3	SPS ERROR
116	11	30	12	3	SPS ERROR
116	14	4	14	45	SPS ERROR
119	15	58	17	23	SPS ERROR
119	23	59	24	0	SPS ERROR
120	0	0	0	52	SPS ERROR
120	2	42	5	59	SPS ERROR
120	21	13	22	7	SPS ERROR
123	2	32	8	47	SPS ERROR
128	0	53	5	24	SPS ERROR
134	3	29	4	48	SPS ERROR
134	10	18	10	50	SPS ERROR
135	8	33	8	53	SPS ERROR
137	14	25	17	45	SPS ERROR
138	22	22	24	0	SPS ERROR
139	0	0	0	3	SPS ERROR
139	6	40	7	10	SPS ERROR
139	9	53	10	42	SPS ERROR
139	10	54	19	51	SPS ERROR
139	22	23	24	0	SPS ERROR
140	0	0	13	18	SPS ERROR
142	10	21	10	40	SPS ERROR
143	2	27	6	16	SPS ERROR
143	8	1	10	19	SPS ERROR
143	11	30	16	47	SPS ERROR
143	18	0	24	0	SPS ERROR
144	0	0	1	24	SPS ERROR
144	11	15	13	18	SPS ERROR
144	14	12	14	27	SPS ERROR
144	14	35	18	0	POWER BREAK
144	22	52	24	0	SPS ERROR
145	0	0	6	15	SPS ERROR
146	9	58	10	19	SPS ERROR
146	14	50	15	8	SPS ERROR
146	18	25	19	7	SPS ERROR
146	19	25	21	2	SPS ERROR
147	11	51	12	31	SPS ERROR
147	13	7	13	23	SPS ERROR
148	12	26	24	0	SPS ERROR
149	0	0	4	25	SPS ERROR
149	19	21	20	52	SPS ERROR
149	23	17	24	0	SPS ERROR
150	0	0	6	4	SPS ERROR
150	7	44	9	0	SPS ERROR

Table II.1.1 (page 1 of 3)

LIST OF BREAKS IN DP PROCESSING THE LAST HALF-YEAR

DAY	START		STOP		COMMENTS.....
150	10	54	12	30	SPS ERROR
150	12	40	16	2	SPS ERROR
151	4	6	7	42	SPS ERROR
151	15	32	17	25	SPS ERROR
151	23	26	24	0	SPS ERROR
152	0	0	0	11	SPS ERROR
152	0	42	10	57	SPS ERROR
152	19	23	21	0	SPS ERROR
154	0	53	6	48	SPS ERROR
154	7	36	11	6	SPS ERROR
154	13	1	13	13	SPS ERROR
154	16	1	16	11	SPS ERROR
155	1	43	8	4	SPS ERROR
156	8	51	10	53	SPS ERROR
156	12	8	13	48	SPS ERROR
156	16	5	19	20	SPS ERROR
156	20	36	24	0	SPS ERROR
157	0	0	8	58	SPS ERROR
157	23	34	24	0	SPS ERROR
158	0	0	0	6	SPS ERROR
158	7	58	9	28	SPS ERROR
158	13	26	15	33	SPS ERROR
159	19	18	20	12	SPS ERROR
161	0	18	18	45	FIRE IN COMPUTER
161	20	21	24	0	SPS ERROR
162	0	0	12	12	SPS ERROR
164	12	10	13	37	SPS ERROR
165	16	24	18	18	CPU ERROR
166	23	47	24	0	SPS ERROR
167	0	0	1	21	SPS ERROR
167	5	21	7	27	SPS ERROR
167	8	19	8	30	SPS ERROR
167	19	39	20	38	SPS ERROR
168	2	55	9	2	SPS ERROR
169	8	2	9	18	SPS ERROR
169	20	33	21	17	SPS ERROR
170	11	39	12	12	C.E. WORK
171	6	1	8	52	SPS ERROR
173	6	7	7	16	CPU ERROR
173	8	4	8	20	SPS ERROR
174	10	53	15	26	CPU ERROR
175	0	26	6	3	CPU ERROR
175	10	44	13	54	C.E. WORK
176	0	6	12	45	CPU ERROR, C.E. WORK
177	6	42	11	55	C.E. WORK
177	20	41	21	47	SPS ERROR
179	10	13	11	48	SPS ERROR
180	7	30	7	50	SPS ERROR
180	8	27	8	35	SPS ERROR
180	20	20	21	17	SPS ERROR
182	6	42	6	51	SPS ERROR
184	7	16	7	27	SPS ERROR
185	16	53	17	48	SPS ERROR
186	3	24	10	51	SPS ERROR
186	13	41	15	47	SPS ERROR
187	10	57	11	37	SPS ERROR
187	16	22	17	19	SPS ERROR
188	4	32	6	47	CPU ERROR
188	7	13	7	31	SPS ERROR
189	12	47	12	58	SPS ERROR
190	3	21	6	44	SPS ERROR
190	14	15	14	24	SPS ERROR
191	8	51	9	4	SPS ERROR
191	11	16	11	28	SPS ERROR
191	19	2	19	48	SPS ERROR
191	22	0	24	0	CPU ERROR
192	0	0	2	0	CPU ERROR
192	7	3	9	36	SPS ERROR
192	15	0	17	8	POWER BREAK
193	14	41	19	3	SPS ERROR
193	23	59	24	0	POWER BREAK
194	0	0	8	7	POWER BREAK

Table II.1.1 (page 2 of 3)

LIST OF BREAKS IN DP PROCESSING THE LAST HALF-YEAR

DAY	START		STOP		COMMENTS.....
194	8	17	8	48	SPS ERROR
194	8	55	9	41	SPS ERROR
194	10	9	11	17	SPS ERROR
194	14	13	14	31	SPS ERROR
195	4	42	5	53	SPS ERROR
195	7	55	8	5	SPS ERROR
200	1	14	2	44	CPU ERROR
202	19	16	20	0	CPU ERROR
202	22	19	24	0	CPU ERROR
203	0	0	6	24	CPU ERROR
204	6	57	7	9	CPU ERROR
205	13	42	14	59	SPS ERROR
205	15	17	17	47	POWER BREAK
207	17	26	17	35	CPU ERROR
208	8	50	9	0	CPU ERROR
210	12	5	13	13	CPU ERROR
214	0	10	7	12	CPU ERROR
214	7	40	9	13	CPU ERROR
216	14	58	17	30	CPU ERROR
218	17	1	18	11	CPU ERROR
220	20	54	21	43	CPU ERROR
222	11	52	12	7	PROG ERROR
223	10	2	12	36	POWER BREAK
224	8	20	13	15	C.E. WORK
225	10	37	10	53	C.E. WORK
225	17	28	19	27	CPU ERROR
226	17	0	18	37	CPU ERROR
227	4	7	13	29	POWER BREAK
229	20	58	21	40	CPU ERROR
229	21	52	22	7	CPU ERROR
231	18	14	20	46	CPU ERROR
232	0	52	6	48	CPU ERROR
233	7	44	7	54	SPS ERROR
234	9	12	10	54	CPU ERROR
234	11	8	11	19	CPU ERROR
235	21	15	24	0	MT ERROR
236	0	0	6	30	MT ERROR
236	12	27	24	0	CPU ERROR
237	0	0	10	7	CPU ERROR
237	10	39	10	59	SPS ERROR
238	7	50	8	9	CPU ERROR
238	12	30	12	48	CPU ERROR
238	18	6	19	12	CPU ERROR
241	19	40	20	14	CPU ERROR
242	2	54	7	32	CPU ERROR
242	15	58	16	41	CPU ERROR
243	7	53	8	40	POWER BREAK
243	8	40	14	40	C.E. WORK
244	6	1	13	43	C.E. WORK
244	15	33	18	0	CPU ERROR
245	6	51	7	33	POWER BREAK
245	7	33	9	33	C.E. WORK
246	1	8	6	32	MT ERROR
247	9	48	9	55	CPU ERROR
251	11	44	12	15	POWER BREAK
253	23	55	24	0	CPU ERROR
254	0	0	0	54	CPU ERROR
256	22	19	23	10	CPU ERROR
257	8	35	8	53	C.E. WORK
258	17	1	17	13	SPS ERROR
258	22	23	23	18	CPU ERROR
264	12	52	13	2	CPU ERROR
265	10	33	10	47	POWER BREAK
266	20	55	21	42	CPU ERROR
267	6	52	7	2	CPU ERROR
271	13	5	13	44	CPU ERROR
272	14	13	14	18	PROG ERROR
273	9	26	9	45	CPU ERROR

Table II.1.1 (page 3 of 3)

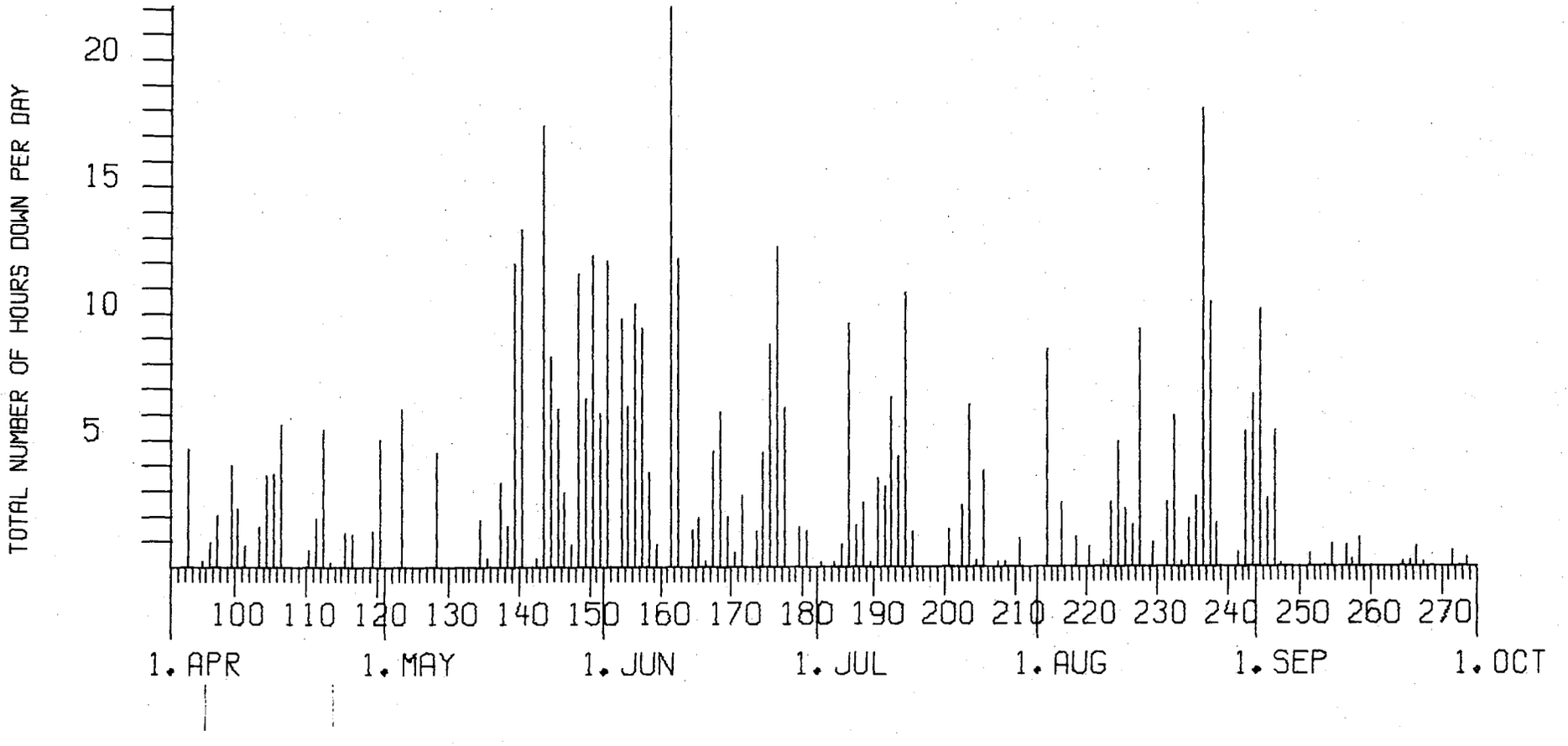

Fig. II.1.1 Detection Processor downtime in the period 1 April - 30 September 1981.

Month	DP Uptime (hrs)	DP Uptime (%)	No. of DP Breaks	No. of Days with Breaks	DP MTBF* (days)
Apr	673.53	93.6	32	19	0.9
May	628.19	84.4	35	18	0.7
Jun	575.72	80.0	40	24	0.6
Jul	683.15	91.8	35	21	0.8
Aug	652.80	87.7	30	22	0.9
Sep	695.45	96.6	19	17	1.5
	3908.84	89.0	191	121	0.9

*Mean-time-between-failures = (Total uptime/No. of up intervals)

TABLE II.1.2

Online System Performance
1 April - 30 September 1981

II.2 Event Processor Operation

In Table II.2.1 some monthly statistics of the Event Processor operation are given:

	Teleseismic	Core Phases	Sum	Daily
Apr 81	264	69	333	11.1
May 81	264	60	324	10.5
Jun 81	243	42	285	9.5
Jul 81	133	77	210	6.8
Aug 81	149	65	214	6.9
Sep 81	215	61	276	9.2
	1268	374	1642	9.0

TABLE II.2.1

B. Kr. Hokland

II.3 NORSAR Data Processing Center (NDPC) Operation

Data Center

During this period all jobs except for DP were run on the new computers; there is no job shop activity, as everyone runs their own jobs from terminals.

A fire in one of the 360 computers on 10 June put that computer permanently out of operation, and the remaining programs that still were dependent on the 360 had to be converted for running on the 4341 computer. It is still necessary for one person to be present in the computer hall to look after the plotters and printers and to mount tapes.

J. Torstveit

II.4 Array Communication

Table II.4.1 reflects the performance of the communications system throughout the reporting period.

In addtion to ordinary irregularities in the communication system, the table also reflects other prominent conditions, such as:

- CTV power failure (high voltage and ripple)
- Line switching between the SPS and the Modcomp processor
- Maintenance visits
- Tests from NDPC
- Cable damage.

In April 01B (NORESS) was frequently used in Modcomp test connection, also 01A was used. 06C was badly affected by a faulty rectifier.

In May 01A and 02C were used for Modcomp tests. 06C was affected by faulty operating rectifier in the CTV. 02C ICW errors observed, but error rate low.

In June 01A, 02C and 03C were used for Modcomp test purposes. 01B (NORESS) and 06C badly affected by cable damage after lightning. 01B (Åsmarka) back in operation (30 June), as 01B (NORESS) still affected by cable repair work.

In July most subarrays were affected one way or another: 01A by cable work and Modcomp test; 01B (NORESS) by formerly reported cable damage; 01B (Årsmarka) loss of data (30 July) Probably cable problem; 02B problems due to power failure; 02C. Spikes on data were reported by data analysts. Errors in ICW's now changed to ODW's (24.7). NTA Lillehammer and Lillestrøm engaged (29.7). Also the NORSAR field maintenance people visited 02C in connection with the spike problem; 03C was affected by cable work between Rena and the SA, and Hamar-Rena; 06C. NTA Hamar continued with cable repair along the cable route after lightning damage.

In August 01A was used in Modcomp tests. 02C ODW's still infested with errors, causing data spikes (errors changed to ODW 24 July) after NTA engagement. 06C cable repair finished by end of the month.

In September between the 17th and 24th, 01B was affected by a faulty 'pupin' coil in a cable. 02B was affected by three different faults: A broken cable, faulty pupin coils in a ground cable, faulty pupin coils in an air cable. On 17 September the EPU power supply was replaced in the 02C CTV. High outage figure (11.4%) has also connection with frequent interruptions due to tests and initiatives to solve the problem.

Table II.4.2 indicates distribution of outages with respect to the individual subarrays. The table also reflects (by asterisks) weeks when some or all subarrays have been affected simultaneously.

II.5 The ARPA Subnetwork

We had incidents in April and September with Loss of Carrier and reduced line quality, but for the remaining months the circuit was quite reliable.

The problems we have faced can be summarized as follows:

Scheduled line break on 12 April. On 27 April 'Carrier Loss'. Pirmasens/Germany reported Loss of Carrier from USA. NCC requested loop tests/modem status on 29 April. Status indicators 'Carrier Loss' and 'Marginal Circuit' initiated

occasionally in May. Loss of Carrier 11 July was corrected in Oslo.

In September the line was down between the 3rd and the 4th due to an irregularity in the USA. The codex modem was tested upon NCC request (40 minutes) in local mode on 22 September. No errors were observed. 'Carrier Loss' observed 25 September. NTA was informed.

II.6 The Terminal Interface Message Processor (TIP)

Apart from a few restarts after power outages 11 & 15 July and 8 Sep, and a faulty Host 3 interface card (10-13 August), reliable performance.

TIP port connections - no change since last report.

O.A. Hansen

Sub-Array	APR (5) (30.3-3.5)		MAY (4) (4.-31.5)		JUN (4) (1.-28.6)		JUL (5) (29.6-2.8)		AUG (4) (3-30.8)		SEP (5) (31.8-4.10)		AVERAGE ½ YEAR	
	>20	>200	>20	>200	>20	>200	>20	>200	>20	>200	>20	>200	>20	>200
01A	1.3	3.9	0.1	20.2	-	12.8	-	2.5	0.1	20.2	-	3.1	0.25	10.4
01B	0.4	67.6	0.2	0.2	-	96.5	-	48.2	0.2	0.2	-	14.1	0.1	37.8
02B	0.2	0.2	6.6	-	7.6	0.5	6.7	16.9	6.6	-	8.1	17.4	6.0	5.8
02C	0.3	0.4	29.8	7.1	0.3	10.1	12.8	3.7	29.8	7.1	21.8	11.4	15.8	6.6
03C	0.4	0.9	0.3	0.4	-	18.5	0.2	57.2	0.3	0.5	0.2	0.1	0.2	12.9
04C	0.2	0.2	4.6	0.3	0.3	5.2	1.7	0.5	4.6	0.3	3.8	0.4	2.5	1.1
06C	11.6	72.3	-	39.6	-	86.7	-	100.0	-	39.6	-	-	1.9	56.4
AVER	2.0	20.8	5.9	16.9	1.1	32.9	3.2	32.7	5.9	9.7	4.8	6.6	3.8	18.7
LESS	06C	01B,06C	02C	01A,06C 03C		01B,03C 06C	02C	01B,03C 06C	02C	01A,06C	02C	01B,02B 02C	02C	01B,06C
	0.5	1.1	1.9	1.6		4.9	1.4	5.9	1.9	1.6	2.0	0.9	1.8	7.5

TABLE II.4.1

Communications (degraded performance >20/outages >200)
Figures in per cent of total time. Month four or five weeks, as indicated.

Week/ Year	Subarray/per cent outage						
	01A	01B	02B	02C	03C	04C	06C
* 14/81	2.3	88.7	-	-	-	-	92.1
* 15	-	100.0	-	-	-	-	100.0
* 16	1.4	100.0	0.7	1.1	0.9	0.9	74.3
* 17	15.5	42.8	-	0.2	2.8	-	79.8
18	0.2	6.6	0.2	0.2	0.7	0.2	15.3
19	-	9.1	-	35.0	-	-	1.5
20	-	9.6	-	100.0	-	-	9.1
21	-	24.2	-	71.4	-	-	25.1
22	0.5	-	-	86.9	-	2.4	-
23	-	85.9	1.8	3.0	1.4	-	47.0
24	-	100.0	0.4	37.5	-	-	100.0
25	-	100.0	-	0.7	4.0	2.0	100.0
26	51.2	100.0	-	0.5	67.8	19.0	100.0
27	12.3	21.6	0.4	1.3	100.0	1.5	100.0
28	-	0.6	-	0.4	100.0	-	100.0
29	0.4	58.1	-	-	85.7	-	100.0
30	-	89.1	22.3	30.5	0.2	1.1	100.0
31	-	71.4	61.8	17.1	-	0.2	100.0
32	46.3	0.5	-	14.6	0.4	0.7	100.0
33	33.5	0.2	-	11.2	0.2	0.2	7.4
34	-	-	-	2.1	-	-	43.6
35	0.9	-	0.2	0.5	0.9	0.2	7.3
36	-	-	-	11.7	-	-	-
37	15.5	0.3	0.1	7.8	0.4	0.9	-
38	-	36.7	-	9.0	-	2.4	-
39	-	33.4	1.5	13.7	0.4	1.2	-
40	-	-	85.7	13.9	-	-	-

TABLE II.4.2

III. IMPROVEMENTS AND MODIFICATIONS

III.1 NORSAR On-line System

Several problems with the new operating system, VM/SP, on IBM 4331 have been overcome, and detection processing using subarray 02C has been tested. During weekend testing of the new system, we experienced 43% CPU load on 4331, with an uptime of 99.99995%. The small loss of data is due to a few single time-outs on the communication controller 2701 between MODCOMP and 4331. We are working with this timing problem to achieve no loss of data as long as the computers are operational. The operational uptime of the computers is determined mostly by AC power uptime. Unpredicted power breaks have caused a few hardware problems on the IBM computer. Whenever a hardware error is detected, the typical repair time is 2-4 hours, including any wait-time on normal working days.

The new IBM 3370 disks had some initial problems with 'disk crash', but these problems are now, according to IBM, eliminated. We have therefore an expected uptime of 99.99, excluding power breaks. Recording of data will be performed by the 4341 computer, where data from the last 24 hours of processing is retrieved from shared disks and written to magnetic tape. A major improvement here will be to use the higher 6250 BPI density tapes, with capacity of 16 hours of NORSAR data on one single reel. An improvement of NORSAR's tape recording equipment is now crucial, since the old IBM tape drives are getting more and more problematic to use.

III.2 NORSAR Event Processor

The processing of EPX records on the detection log tapes is heavily automated using the AUTOEP program. The analysts have found it most practical to produce offline plots, where the events to plot are automatically selected by criteria in AUTOEP. The plots are then reviewed and the analysts have now a new rerun program using high rate tape input. Processing time is small and repeated processings are easily performed by use of disk files. With the new online system operational, the EPX data will be retrieved from shared disk, and reruns may also be performed rapidly having 24 hours of the latest online data on disk. Refinements of the processing will be developed using the graphic display terminals.

III.3 Program Developments

All of the mostly used application programs are converted to the new standards, and several new programs have been developed. It is typical for program development time and testing using the new computers that many find it quicker to develop a new program rather than look for the old card-deck and use that. Since test time is significantly decreased, the programs are more rapidly getting reliable status, more data may be analyzed and the results are getting better. We are building up data bases on disk both for instrument data and bulletin data. A file in the VM/CMS system is identified by name and type. We have now a system where instrument data files have the basic information in the file identification, i.e., a file containing NORSAR data from 1981, DOY 256, start time 12.56.23 will be identified by file name 'NA081256' and file type '125623'. In addition we may put a record in the beginning of the file describing the data, such as a bulletin card for an event. Several programs are developed using such data files. Moreover, there are new programs for bulletin sorting, map plotting, data plotting, and all programs are online available to everybody.

J. Fyen

III.4 Improvements and Modifications

The changes of the array stations in the period 1 April to 31 October 1981 are given in Table III.4.2. The 'Old NORESS' was disconnected due to difficulties in restoring the communication line after thunderstorm damage in the beginning of June, and the original subarray configuration 01B was reconnected as of 30 June 1981. The attenuated (-30 dB) channel 01A04 was damaged by lightning 23 June and has been down from that date. The analog channel 06C02 has been down since 7 September due to fault on the Helicorder. Table III.4.1 gives the cross reference of the NORESS channels after a new numbering of the stations was introduced as of 30 October, refer Fig. III.4.1. The data signal before filtering of eight of these channels are multiplexed on a new telephone line and sent as analog data to NDPC for analog-to-digital conversion and processing in the Modcomp computer.

NORESS Seismometer Station No. (Ref. Fig. III.4.1)	Previous 06C(new)/ 01B(old) NORESS channels	06C New SLEM channels	Analog channel no. at NDPC
1	06C01		1
2	06C02	02	
3	06C06		2
4	06C03		3
5	06C06		4
6	06C04	03	6
7	06C05		5
8	01B03	04	7
9	01B04	05	8
10	01B01	01	
11	01B05	06	
12	01B02		

Table III.4.1

NORESS seismometer and channel numbering as of 30 October 1981 with cross reference to previous numbering.

Two Kinemetrics PDR-2 digital 6-channel field systems were acquired last July and have been used for noise measurements at several places in Norway and Finland. Also a Kinemetrics CCS-1 Compuseis communication system has been received and installed at NDPC for playback of PDR-2 cassettes and possible communication interface for the PDR-2

A.Kr. Nilsen

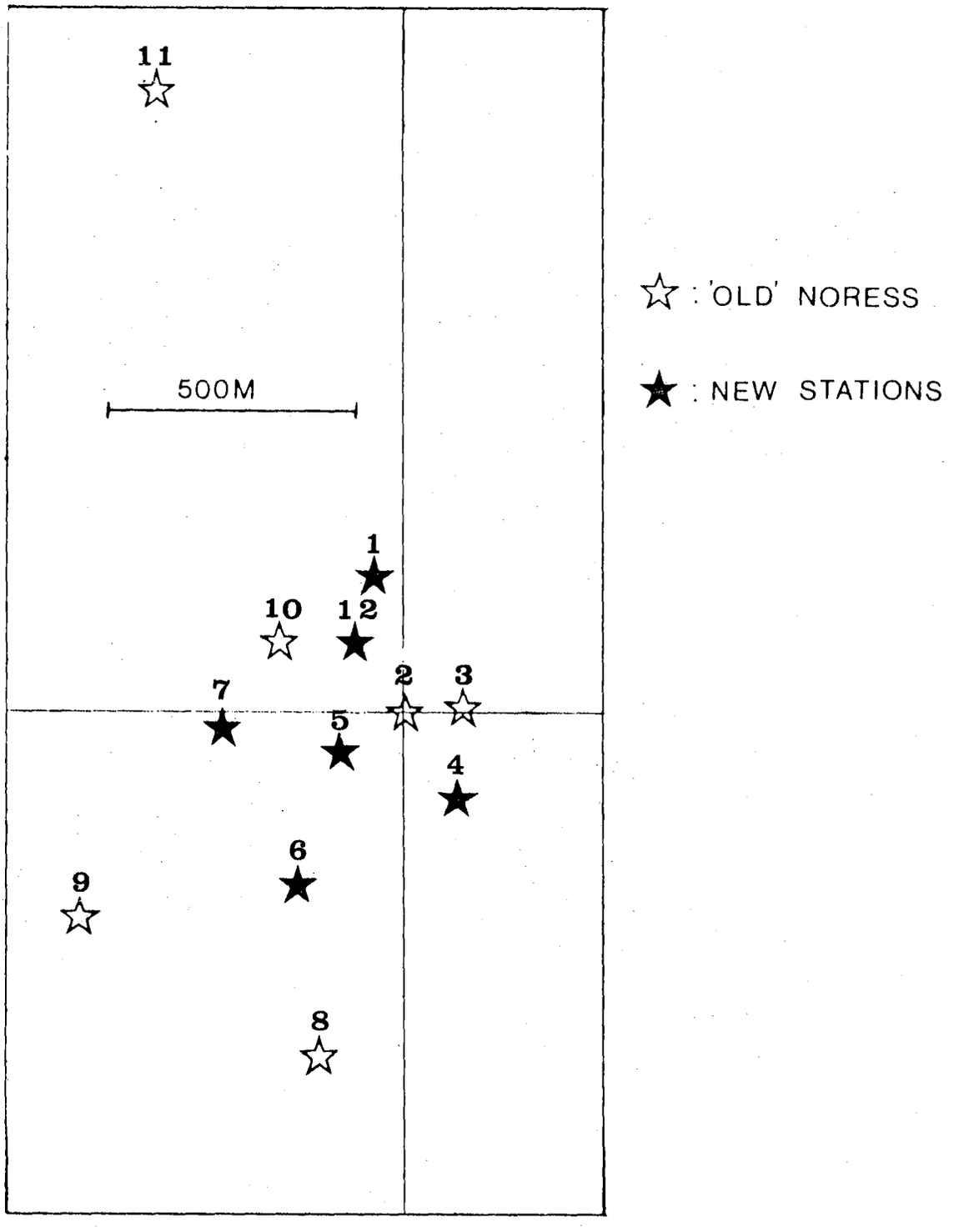

Fig. III.4.1 NORESS seismometer station numbering from 30 October 1981.

Subarray Normally	Instr. No. within SA	Ch. No. on NORSAR Data Tape	Time of Change			
			06/30/81	06/23/81	07/29/81	10/30/81
01A	1	1		-		
(1)	2	2		-		
	3	3		-		
	4	4		Attn.ch. down		
	5	5		-		
	6	6		-		
01B	1	7	Normal SA config.	(1)		
(2)	2	8		(2)		
	3	9		(3)		
	4	10		(4)		
	5	11		(5)		
	6	12		(6)		
02B	1	13				
(3)	2	14				
	3	15				
	4	16				
	5	17				
	6	18				
02C	1	19			-	
(4)	2	20			-	
	3	21			-	
	4	22			-	
	5	23			-	
	6	24			8 Hz filter out 4.75 Hz filter in	

TABLE III.4.2

Status of NORSAR SP instruments recorded on data tape.
(Page 1)

Subarray Normally	Instr. No. within SA	Ch. No. on NORSAR Data Tape	Time of Change				
			06/30/81	06/23/81	07/29/81	10/07/81	10/30/81
03C	1	25					
(5)	2	26					
	3	27					
	4	28					
	5	29					
	6	30					
04C	1	31					
(6)	2	32					
	3	33					
	4	34					
	5	35					
	6	36					
06C	1	37				Normal SA conf.(1)	Previous ch. 01B01*
(7)	2	38				" (2)	" 06C02*
	3	39				" (3)	" 06C04*
	4	40				" (4)	" 01B03*
	5	41				" (5)	" 01B04*
	6	42				" (6)	" 01B05*
							* NORESS data

TABLE III.4.2
(Page 2)

IV. FIELD MAINTENANCE ACTIVITY

Parts of array monitoring have been somewhat deteriorated in this period after the interactive read/write program (ARSTAT) on array status file (ASF) located on the DP shared disk was interrupted by removing the IBM 2260 terminal and its controller. Temporary programs for read/write on ASF are now in use. Permanent programs will be implemented in the new DP program package. As in previous periods the array field instrumentation performance has been satisfactory, but thunder storms have also this summer caused damage on electronics and communication lines. Most of the well head vaults' wooden covers in the A- and B-ring have been replaced during the summer, and much work has been done with subarray 02B extension; at least four seismometer stations will be set in operation this year.

Maintenance Visits

Table IV.1 gives the number of visits to the NORSAR subarrays. The average number of visits to each subarray is 5.9, which equals the visits for the last reporting period.

Subarrays	01A	01B	02B	02C	03C	04C	06C/NORESS	Total
No. of Visits	8	11	3	2	4	2	11	41

TABLE IV.1

Number of visits to the NORSAR subarrays including NORESS in the period 1 April-30 October 1981

Preventive Maintenance Projects

The preventive maintenance work of the NORSAR array instrumentation is listed in Table IV.2. The adjustments are corrections of characteristics within the tolerance limits before they drift outside the tolerance limits.

Unit	Action	No. of Actions
Seismometer	MP adjust (in field)	7
Line Termination Amplifier	Adjustment of channel gain (SP)	7
	-"- (LP)	3
	-"- of DC offset (SP)	13
Emergency Power	Battery and charger check including refill of water	8
Cleaning of CTV		4

TABLE IV.2

Preventive maintenance work in the period
1 April - 30 September 1981

Corrective Maintenance

The corrective maintenance of the NORSAR array instrumentation, which covers the required adjustments and replacements, is given in Table IV.3.

Unit	Characteristics	SP		LP	
		Repl.	Adj.	Repl.	Adj.
Seismometer	FP (in field)				2
	MP (in field)				7
	MP/FP (at NDPC)				40
	Damping		1		
	RCD			4	
	MP lamps			3	
Seismometer Ampl. RA/5, Ithaco	Gain		1		
	Protection card	4			
	JC-box	4			
Line Termination Amplifier	Gain		8		
	DC offset		2		
	Miscellaneous	1			
SLEM	Test generators	2	2		
	EPU	1			
Power, Charger/ Rectifier	Time relay	2			
	Power supply for MP Lamps			3	
Replacement of WHV wooden cover		13			
Other constructions		6			

TABLE IV.3

Total number of required adjustments and replacements of NORSAR field equipment in the period 1 April - 30 September 1981.

Power Breaks, Cable Breakages, Communications Faults

One power break required action of the field crew, that is, assistance to the local power company. Six SP cables were repaired, and communication faults were corrected six times by our field crew.

Array Status

There is little change in the status of the array instrumentation compared with previous periods. As of 30 September 1981 five channels had out-of-tolerance conditions (01A04; 01B04,05; 03C06; 06C06). Channels with nonstandard conditions are:

01A	02,03	NS and EW horizontal SP
06C	01-06	NORESS

Four channels have 8 Hz filters (standard 4.75 Hz): 01A06, 02B06, 03C06 and 04C06.

A.K. Nilsen

ABBREVIATIONS

CTV	-	Central Terminal Vault
DC	-	Direct current
DP	-	Detection Processor
EPU	-	External Power Unit
EW	-	East-West
FP	-	Free period
LP	-	Long period
MP	-	Mass position
NDPC	-	NORSAR Data Processing Center
NORESS	-	NORSAR Experimental Small-Aperture Subarray
NS	-	North-South
RCD	-	Remote centering device
SLEM	-	Seismic short and long period electronics module
SP	-	Short period
WHV	-	Well Head Vault

V. DOCUMENTATION DEVELOPED

Doornbos, D.J., 1981: Seismic moment tensors and kinematic source parameters, Geophys. J.R. astr. Soc., in press.

Gjøystdal, H., & B. Ursin, 1981: Inversion of reflection times in three dimensions, Geophysics, 46, 972-983.

Nilsen, A.K., 1981: Semiannual Technical Summary, 1 October 1980-31 March 1981, NORSAR Sci. Rep. No. 2-80/81, NTNF/NORSAR, Kjeller, Norway

Sandvin, O., & D. Tjøstheim, 1981: A numerical comparison of two criteria for determining the order of AR processes, Math. Operationsforsch. Statis. Vol. 12, No. 1, 1-9.

Troitskiy, P., E.S. Husebye & A. Nikolaev, 1981: Earth holography experiment - Lithospheric studies based on the principles of holography, Nature, 294, 618-623.

VI. SUMMARY OF TECHNICAL REPORTS/PAPERS PREPARED

VI.1 Constrained inversion for sources of finite extent

In the previous Semiannual Summary we reported on the representation of seismic response in terms of 20 source parameters which are related to components of the moment tensors, and which are also related to the parameters of finite fault models. The usual representation in terms of 6 components of the zero degree moment tensor is adequate for point sources at given location. For point sources at unknown location, a 10 parameter representation (including first degree moments) is necessary and adequate, and the location may be determined (Dziewonski et al, 1981). For sufficiently extended sources, the 20 parameter representation (including second degree moments) is necessary; from an investigation of classical Haskell and Savage type of fault models it is estimated that for sources with $M_S>6$, the relative contribution of second degree moments may be of the order of 10% or more, even in long-period seismograms. The representation is adequate as long as source rise time and spatial extent are smaller than seismic wave period and wave length.

Parameters related to second degree moments can be interpreted in terms of source rise time, orientation and spatial extent, and average rupture velocity. Orientation of the source region can also be inferred, in part, from the zero degree moments. Thus, solutions for the different source parameters should be mutually consistent. Furthermore, values for some of the parameters should be positive or, more specifically, be in a range of 'acceptable' values dictated by our conception of the mechanism of faulting. Previously we reported that not all of the above criteria were fulfilled by the results of an inversion of SRO data from a deep event in the Bali Sea. Thus, it appears necessary to impose (generally non-linear) constraints on the solution. We have now obtained the contraints in a linearized form, to be included in the inversion procedure. Moreover, since the constraints are precisely those appearing as a priori assumptions in the conventional methods of source analysis, it is also possible to investigate the impact of these assumptions. Table VI.1.1 and Fig. VI.1.2 summarize a comparison of results of constrained and unconstrained inversion for the Bali Sea event. Case number 1 in this table assumes a point source, and no constraints are necessary. Case number 3 assumes a plane fault,

which can be represented by just one double couple. Although the solution for this case seems 'reasonable' (partly because of the constraints so imposed), it should be noted that the RMS error is about the same as for the point source solution, case number 1. Since the latter involves less degrees of freedom, it would be preferred from a statistical point of view. The point source solution does not completely specify a single double couple, hence the corresponding fault is not necessarily plane. This raises a question about the effect of the plane fault assumption in source analysis. Another question concerns the effect of errors (or anomalies) in the data. To investigate these problems we computed synthetic seismograms for the point source solution (displayed in Fig. VI.1.1), and these syntheses formed the basis of a number of inversion experiments, also summarized in Table VI.1.1 and Fig. VI.1.2. From these experiments we conclude that unjustified assumption of a plane fault may lead to overestimate the fault surface area. The same is true if the data are corrupted by errors (or anomalies). The significance of the effect depends on the relative excitation factors of the source parameters. It should be realized that this effect is not a consequence of the moment tensor representation; it is to be expected in any method of source analysis. In the moment tensor formulation however, the plane fault assumption can be avoided.

D.J. Doornbos

References

Doornbos, D.J., 1981: Seismic moment tensors, in 'Identification of Seismic Sources', eds. E.S. Husebye and S. Mykkeltveit, D. Reidel Publ. Co.

Doornbos, D.J., 1982: Seismic moment tensors and kinematic source parameters, Geophys. J.R. astr. Soc., in press.

Dziewonski, A.M., T.A. Chou and J.H. Woodhouse, 1981: Determination of source mechanism and hypocentral coordinates from waveform data, in 'Identification of Seismic Sources', eds. E.S. Husebye and S. Mykkeltveit, D. Reidel Publ. Co.

Table VI.1.1 Results of inversion with constraints, for Bali Sea event of 1978, June 10. M and N are scalar moments of major and minor double couple, $\Delta(\tau^2)$ is temporal moment of degree two, $\bar{v}$ is average rupture velocity, a^2, b^2, c^2 are eigenvalues of source ellipsoid. Standard deviations in parentheses Fault constraints as discussed in the text, and given explicitly in Doornbos (1982).

Nr	Data	Fault	M	N	$\Delta(\tau^2)$	$\bar{v}$	a^2	b^2	c^2	RMS
		Constrained	(10^{25} dyne·cm)	(10^{25} dyne·cm)	(s^2)	(km/s)	(km^2)	(km^2)	(km^2)	error
1	Observed	No	1.07 (±0.06)	0.10 (±0.07)	0	0	0	0	0	631
2	Observed	No	1.09 (±0.10)	0.09 (±0.10)	3.23 (±27.14)	45.0 (±75.2)	789.9 (±1120.9)	-3051.9 (±1793.8)	-686.0 (±2489.3)	515
3	Observed	Yes	1.10 (±0.13)	0	0.91 (±1.43)	3.9 (±7.4)	27.6 (±4.7)	1.6 (±4.4)	0	632
4	Synthetic	No	1.07	0.10	0.06	9.9	7.2	-1.2	-1.0	3
5	Synthetic	Yes	1.07	0	0.39	4.4	7.9	2.9	0	59
6	Synthetic*	Yes	1.06	0	0.19	6.9	37.7	4.4	0	56
7	Synthetic**	No	0.93 (±0.05)	0.02 (±0.05)	1.30 (±12.93)	58.7 (±35.8)	1178.8 (±534.2)	-1380.4 (±854.9)	-330.5 (±1186.3)	301
8	Synthetic**	Yes	0.92 (±0.06)	0	1.05 (±0.68)	0.3 (±3.5)	37.1 (±2.2)	0.1 (±2.1)	0	330

* In case number 6, rupture velocity is unconstrained.

** In case number 7 and 8, random errors have been introduced into sythetics.

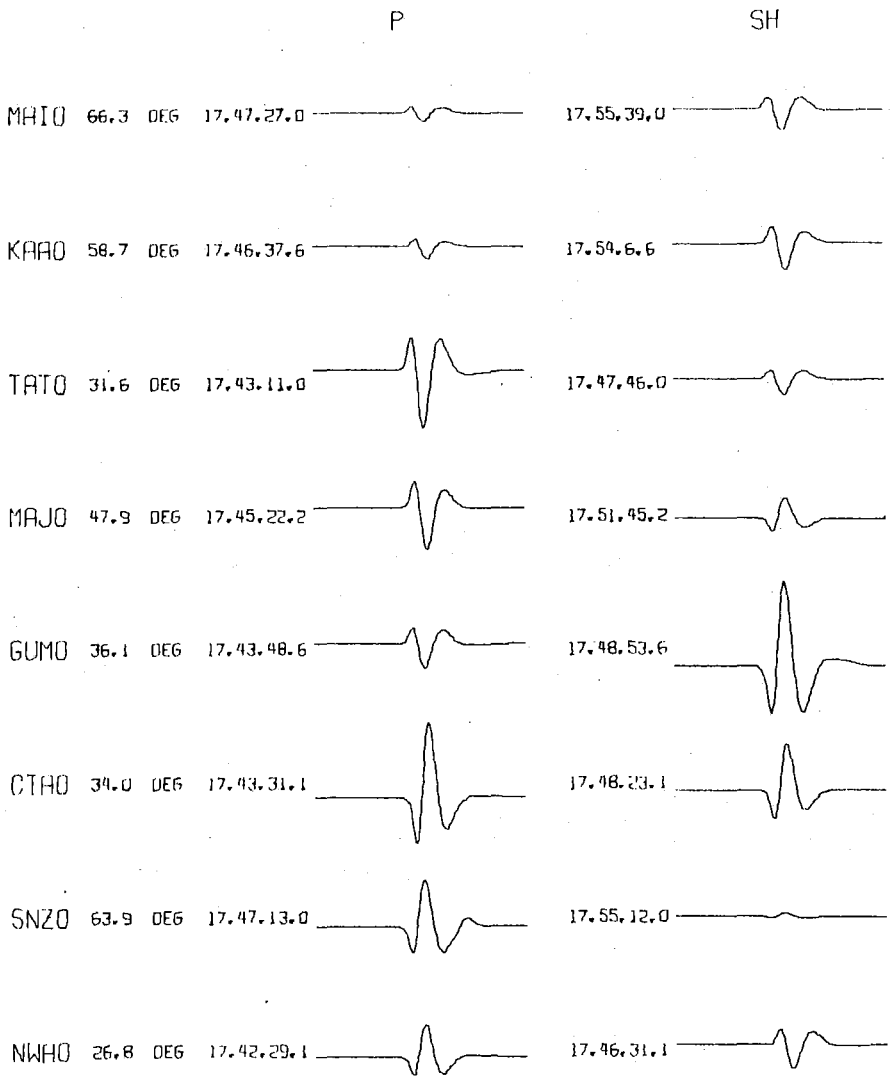

Fig. VI.1.1 Synthetic records with P and SH at SRO and ASRO stations, for a source corresponding to the solution of case number 1 in Table VI.1.1. Record length is 2.5 minutes. Different amplitude scale for different components.

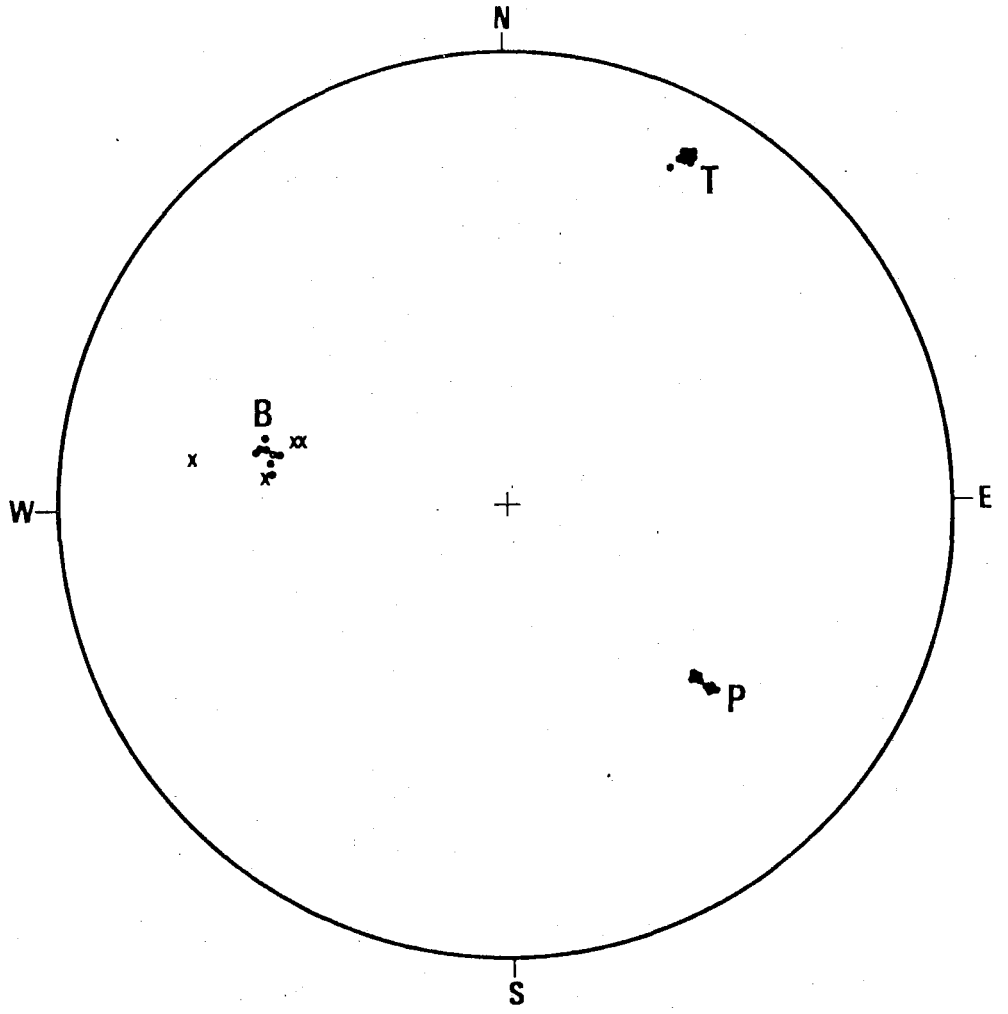

Fig. VI.1.2 Fault plane solutions in equal area projections for the cases in Table VI.1.1. ●: Principal axes of moment tensor of degree zero, x: Major axis of moment tensor of degree two, in cases where fault constraints were imposed.

VI.2 Signal and noise correlations and seismic array configuration optimalization

One of the subtasks under the NORSAR regional seismology research program is to devise an optimal sensor layout for a prototype regional seismic array. This contribution deals with initial attempts at array configuration optimalization based on observations of signal and noise correlations. More specifically, we outline a strategy for maximizing the gain funtion, which is expressible in terms of signal and noise correlations only. Possible constraints due to preferred lobe patterns are not dealt with in this study.

We define signal-to-noise ratio gain from beamforming by

$$G = \sum_{i,j} \rho_{ij} / \sum_{i,j} c_{ij} \qquad (1)$$

where ρ_{ij} is the signal correlation between sensors i and j and c_{ij} the noise correlation. The correlations ρ_{ij} and c_{ij} will, in general, be functions of relative positions of sensors and frequency. In addition, ρ_{ij} depends on the phase type considered.

In the following, we establish models for signal and noise correlations to be used in maximizing the gain in eq. (1).

Signal and noise correlation measurements

Measurements of signal and noise correlations are made from the 12-element NORESS array, described in previous semiannual technical summaries. Thus, predictions on optimum geometries of unimplemented arrays will be based on the correlation measurements made from the existing NORESS array.

From the five regional events in Table VI.2.1 we have identified Pn, Pg and Lg phases, which in turn have been subjected to correlation analysis. Since the original sampling rate is 20 Hz, a resampling at 100 Hz was necessary to achieve more accurate time shifts for the correlation computations. The shifts

were performed with an optimum line-up of correlating peaks in the signals, and 2 sec of each phase were analyzed. The NORESS array with its 12 elements offers 66 different sensor combinations resulting in 66 cross-correlation values for separations ranging from 120 to 1950 m. Correlation values were averaged into separation intervals of 100 m. Also, averaging is performed over all available phases of the same kind. The results for the Pn phase are shown in Fig. VI.2.1 for the five frequency bands given in Table VI.2.2. Figs. VI.2.2 and VI.2.3 show correlation curves for the Pg and Lg phases, correspondingly.

The results for the Pn phase show increasing correlation with frequency. This is due to the high frequency content in the Pn signal; the Pn spectrum peaks at around 4 Hz. The Pg phase exhibits high correlation values throughout the range of both frequency and sensor separation. The Lg phase, on the other hand, correlates poorly for the higher frequencies.

Selected noise records have been subjected to the same kind of correlation analysis, but now with zero shifts. The noise is taken from five time windows, each consisting of 3 consecutive segments of 4 sec each, immediately preceding the first arrival onset time for the events in Table VI.2.1, so averaging is done over a total of 15 time windows. The results are given in Fig. VI.2.4.

The standard deviations associated with the curves in Fig. VI.2.4 are fairly modest, so we must consider the negative cross-correlation values a real entity. Also, it seems justified to consider the cross-correlations a function of interstation separations only, which is of course already implictly assumed in producing Fig. VI.2.4.

Array configuration optimalization

We are now in a position to contruct otpimal arrays by maximizing the gain expression given by eq. (1), utilizing the correlation functions derived from the measurements described above. We are thinking in terms of arrays with 15-20 elements, out of which an optimal subset should be used in the processing of a

particular phase. In fact, the variation of cross-correlations (especially for the noise) with frequency is so strong that one would expect rather drastically different geometries to be optimal for different frequencies. So, realizing the extended range of signal frequencies encountered in regional seismic phases, the optimalization algorithm must be capable of coming up with a final geometry that comprises a broad variety of optimal subsets.

So far, the program for optimizing the gain handles one frequency or a 'weighted' combination of frequencies. Array configuration results based on signal correlations of the Lg wave and the noise are given in Fig. VI.2.5.

The array geometries in Fig. VI.2.5 are generated as follows: The observed correlation curves are represented by analytical functions which are pieced together so as to achieve continuous derivatives. Then a starting configuration is defined and a program which maximizes the gain function by a rapid descent method due to Fletcher and Powell (1963) finds an optimal configuration for the number of sensors in question. The suite of geometries in Fig. VI.2.5 are generated by repeated application of the Fletcher-Powell routine, where the starting geometry for N sensors is defined by the optimal geometry for N-1 sensors, with one sensor added at the point of gravity for the N-1 sensors.

S. Mykkeltveit
K. Åstebøl
D. Doornbos
E.S. Husebye

References

Fletcher, R. and M.J.D. Powell, 1963: A rapid descent method for minimization Computer Journal, 6, 163-168.

Wahlstrøm, R., 1978: Magnitude-scaling of earthquakes in Fennoscandia. Report No. 3-78, Seismological Institute, Uppsala, Sweden.

Date	Origin time	Location		Magnitude M_L
06 Nov 1980	14.53.02	59.5°N	10.7°E	2.1
25 Nov 1980	02.39.49	58.4°N	13.7°E	2.4
29 Nov 1980	20.42.16	51.2°N	18.5°E	3.5
26 Feb 1981	17.43.53	60.3°N	15.9°E	2.1
01 Mar 1981	05.08.16	62.8°N	6.2°E	2.7

Table VI.2.1

Local events used in this study. The local magnitude M_L is computed in accordance with Wahlström (1978).

Filter No.	Bandpass range (Hz)
1	0.8-2.8
2	1.2-3.2
3	1.6-4.0
4	2.0-4.8
5	2.4-4.8

Table VI.2.2

Butterworth bandpass filters (3rd order) used in this study.

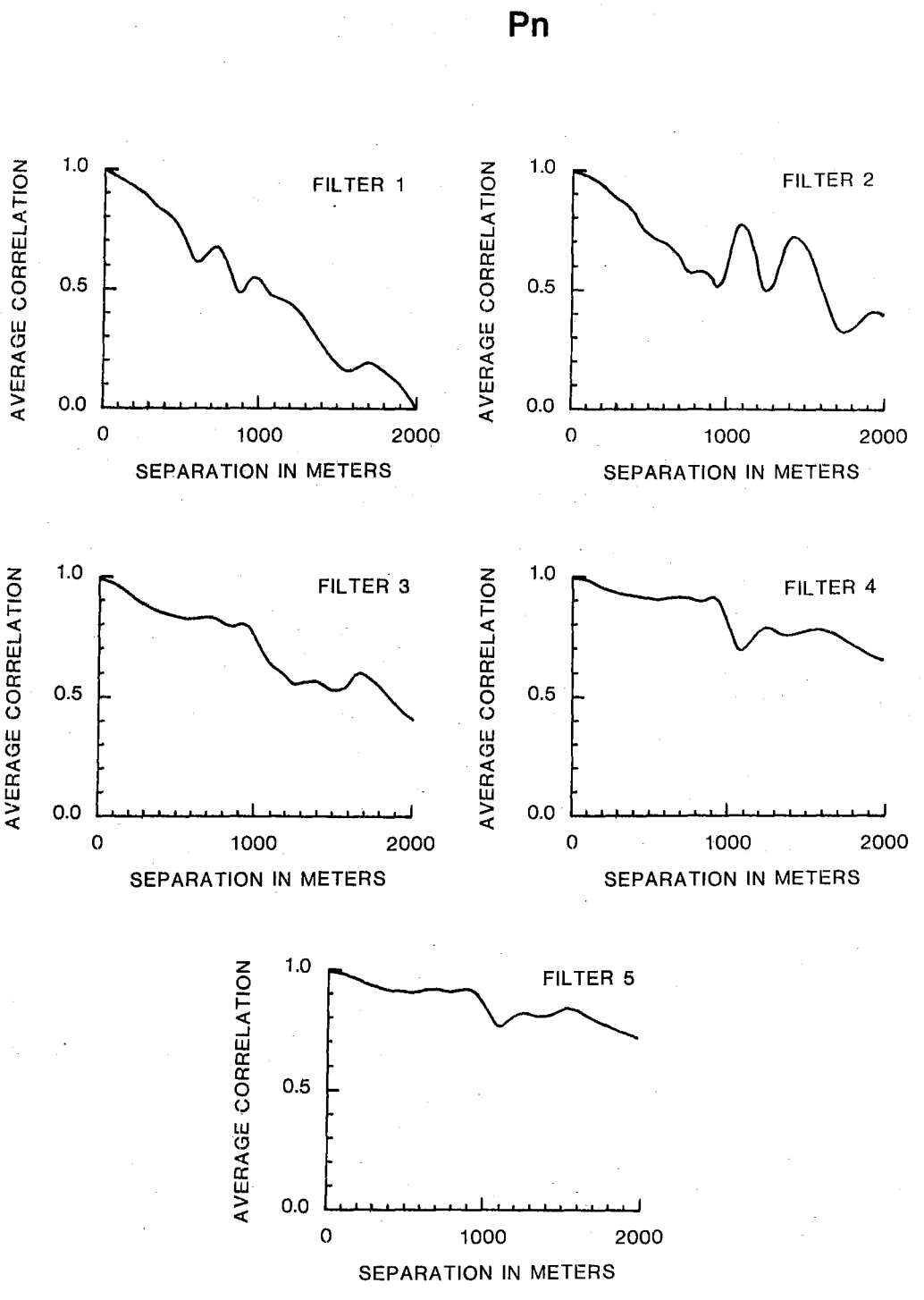

Fig. VI.2.1 Average signal correlations for the Pn phase. Each curve is based on measurements from 66 combinations of stations and averaging is performed within intervals of 100 m. The filters are defined in Table VI.2.2.

Pg

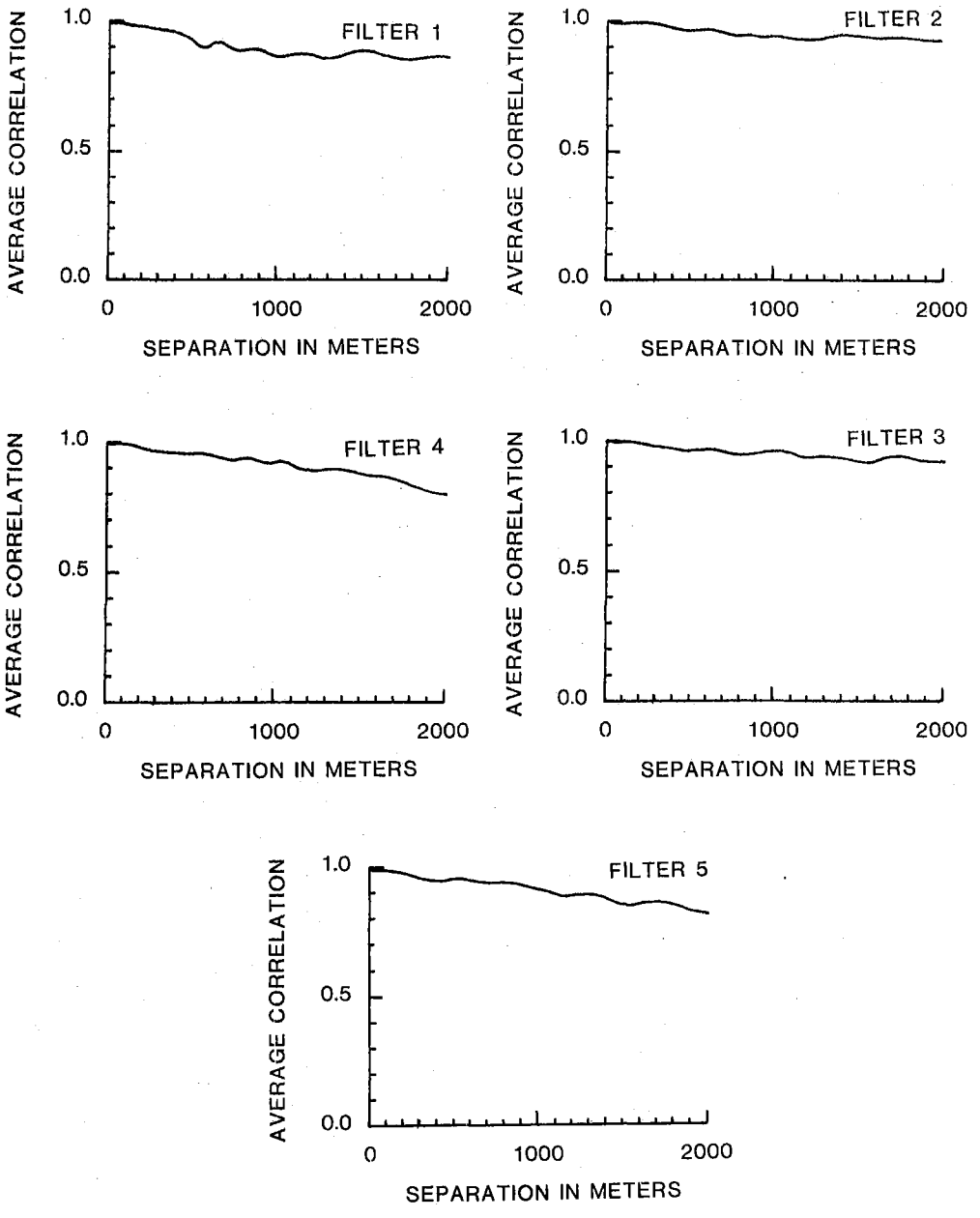

Fig. VI.2.2 Signal correlations for the Pg phase.

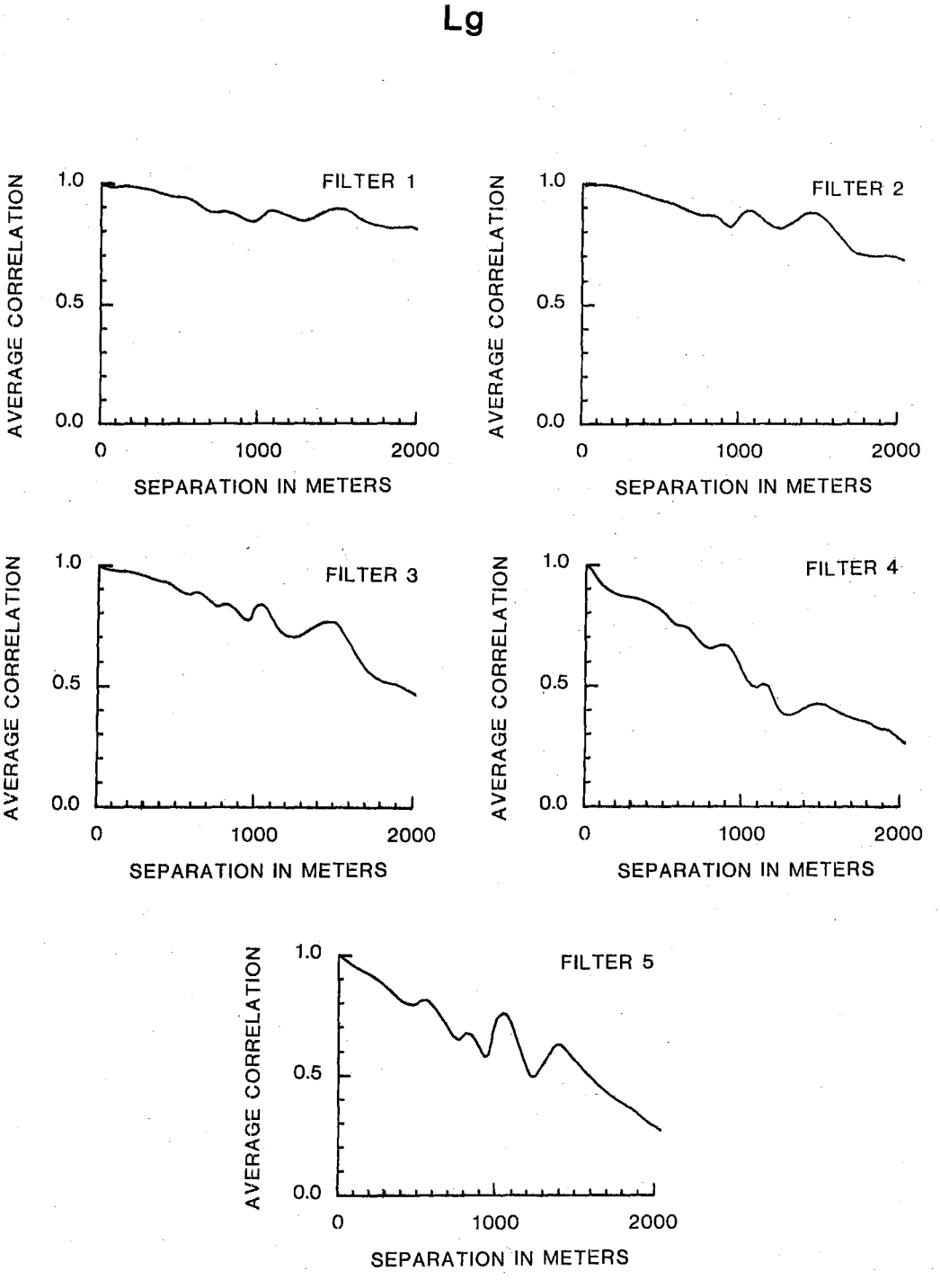

Fig. VI.2.3 Signal correlations for the Lg phase.

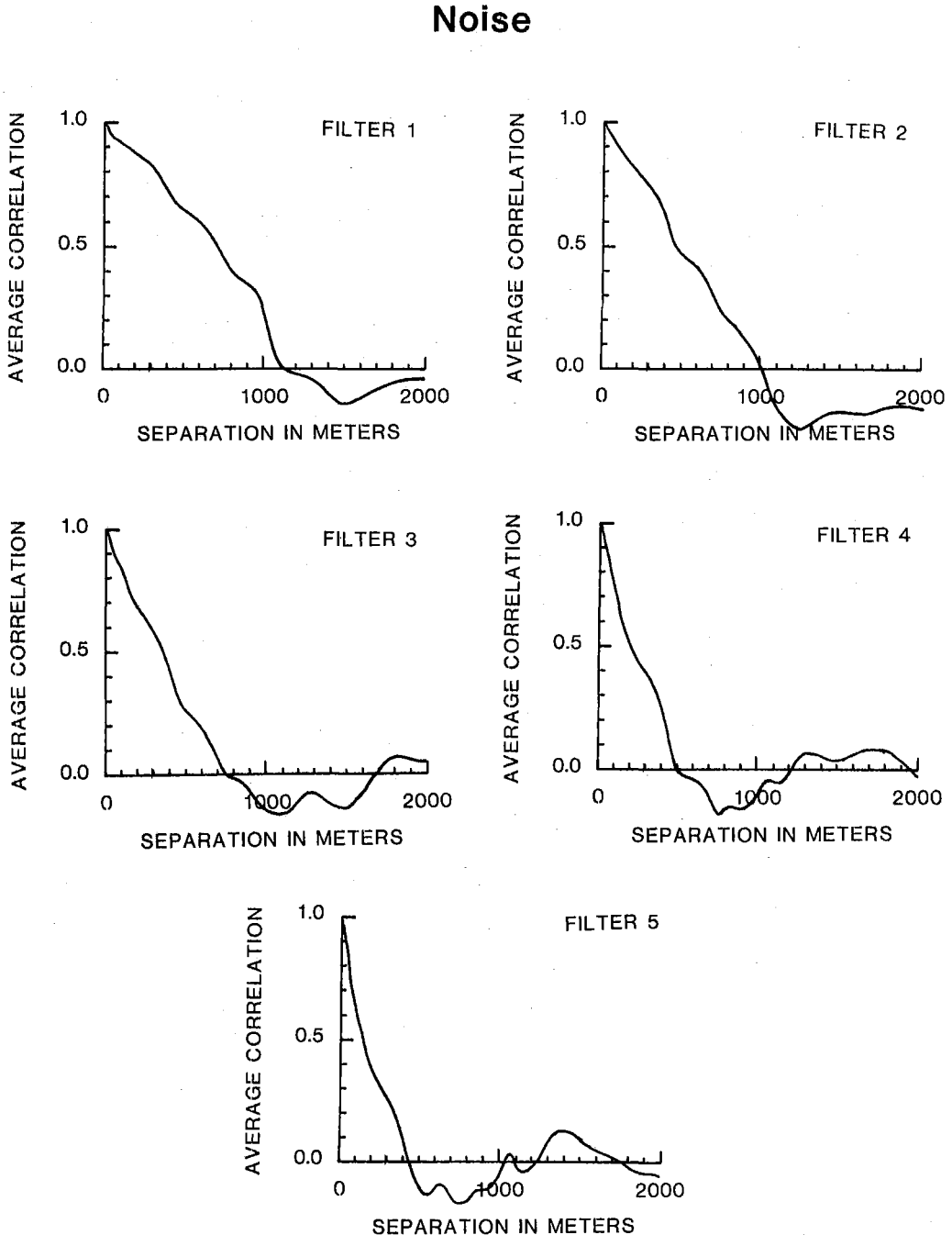

Fig. VI.2.4 Noise correlation results.

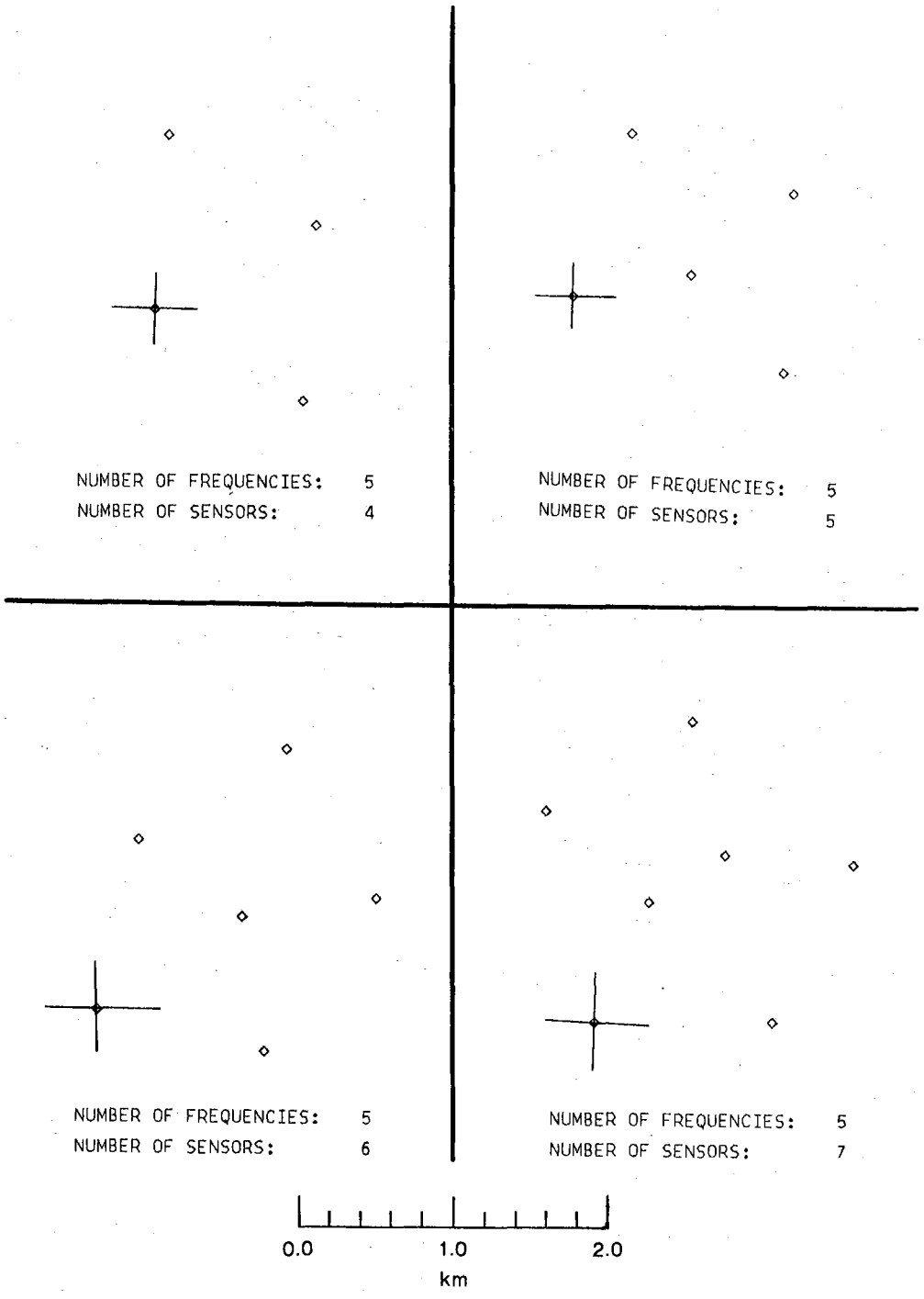

Fig. VI.2.5a Sensor geometries from maximizing the gain function. Equal weight is given to each of the five frequencies in Table VI.2.2. One position, appropriately marked, is kept fixed. This suite of frames shows optimal configurations for 4, 5, 6 and 7 sensors.

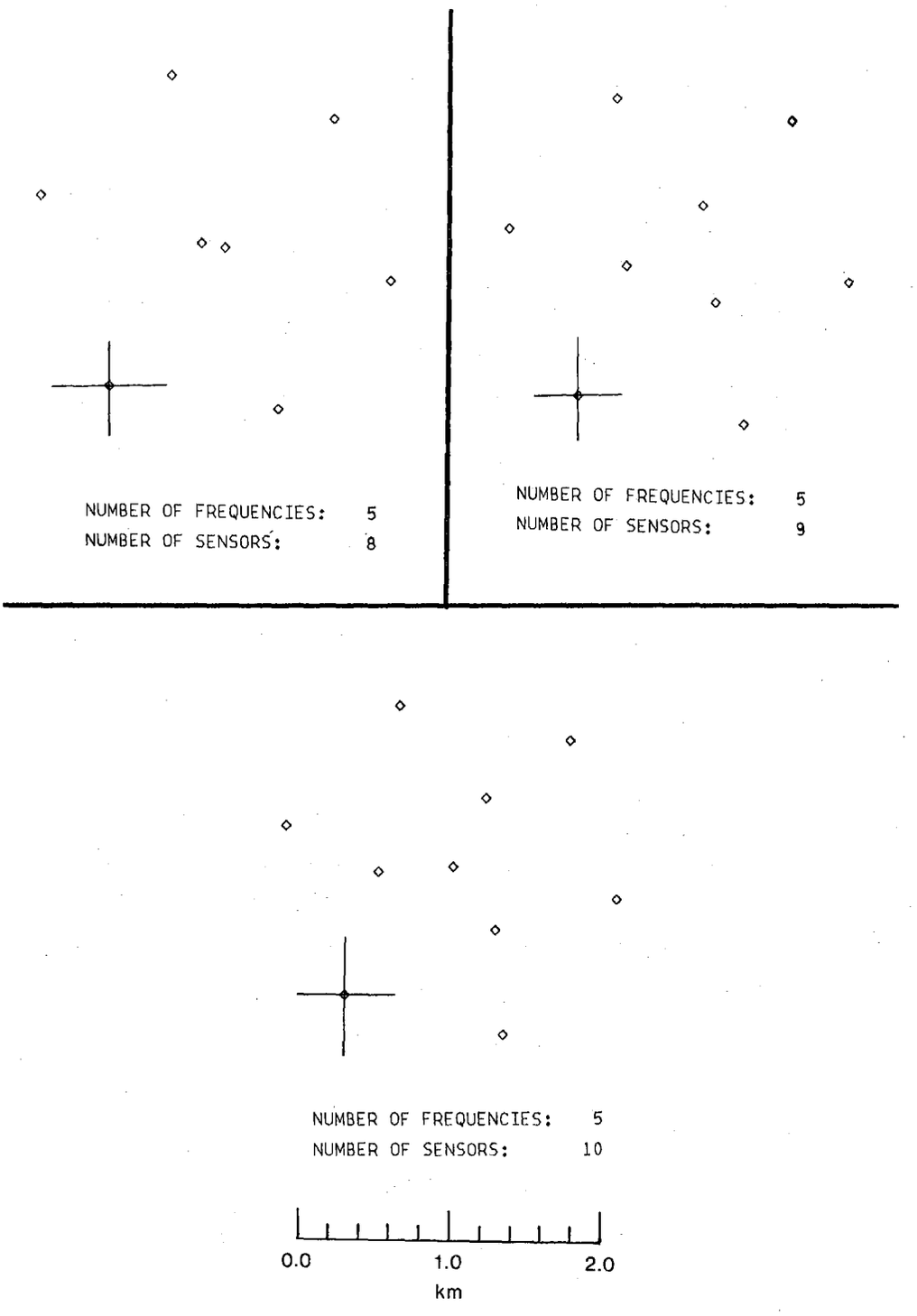

Fig. VI.2.5b Same as Fig. VI.2.5a, but now for 8, 9 and 10 sensors.

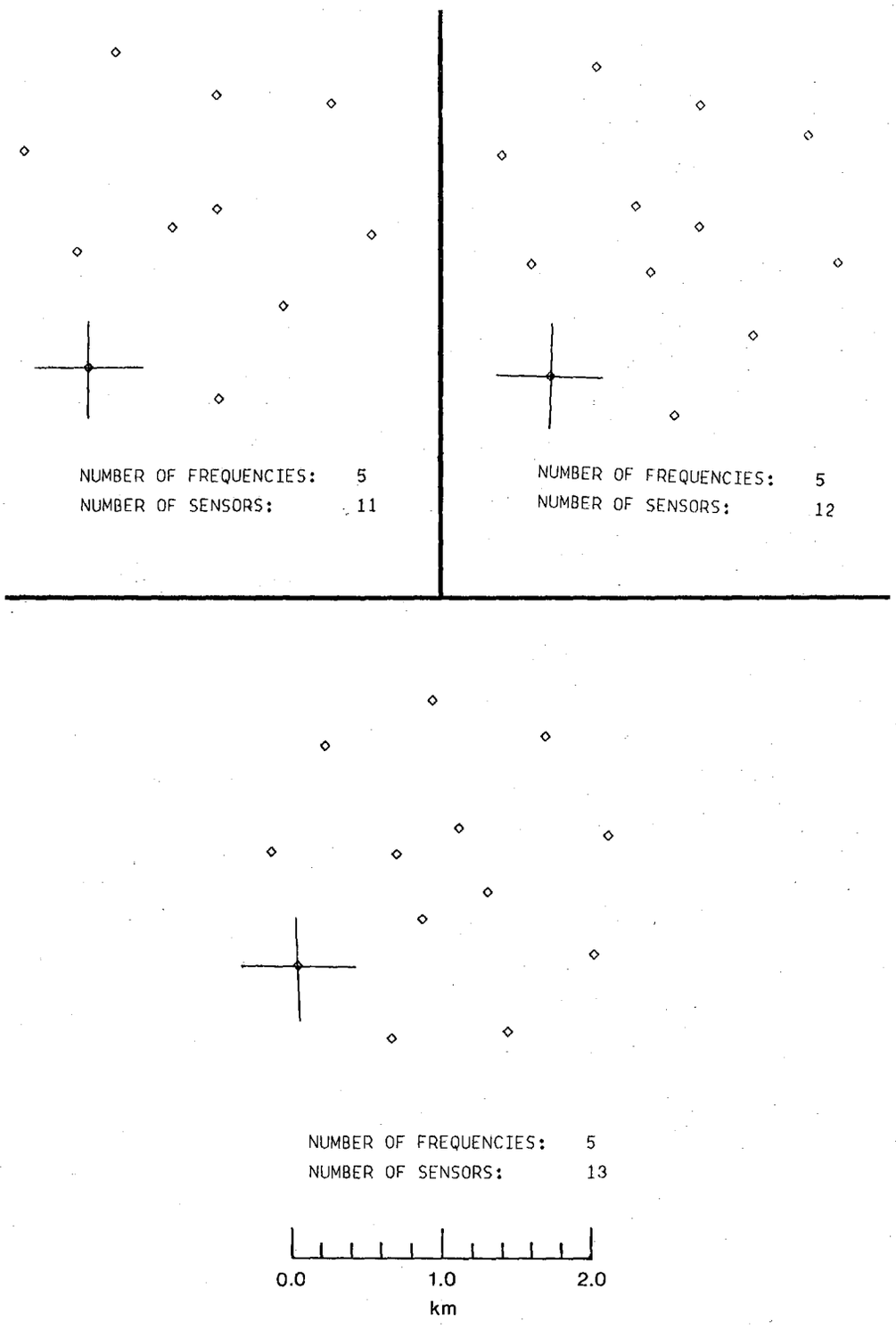

Fig. VI.2.5c Same as Fig. VI.2.5a, but now for 11, 12 and 13 sensors.

VI.3 3-D seismic mapping of the Iceland hot spot

An efficient way of mapping upper mantle structural heterogeneities is that of using the ACH-method (Aki et al, 1977) for inversion of travel time observations from a seismic array or similar kinds of seismograph networks. In the latter cases, the ACH-method has been adapted to handle observations from large-scale networks (aperture ~ 10 deg) in which cases the necessary data easily can be retrieved from the ISC-bulletin tapes (e.g., see Hovland et al, 1981; Gubbins, 1981). This approach for mapping the extent of lateral heterogeneities in the upper mantle has proved to be successful as compared to surface wave dispersion analysis.

In this section we describe an attempt to map seismically the deep structure beneath Iceland using available P-travel time residuals from the local seismograph network (see Fig. VI.3.1). This problem is an interesting one from a tectonic point of view, as evidence for deep-seated roots (down to 300-400 km) of hypothesized hot spots like Iceland and Hawaii have not been presented to our knowledge. Indeed, recently Anderson (1981) argued that the depth extent of hot spots should be confined to the uppermost 200 km (lithosphere) of the mantle.

Data and method of analysis

The travel time observations used in this inversion experiment were taken (read) from original seismogram records of the Icelandic network comprising altogether 39 stations. In the time interval 1974-80 the total number of events available for analysis was about 160, out of which 61 were found useful. The event selection criteria imposed were that a minimum of 5 stations exhibited reasonably clear P-wave recordings, and besides that the azimuth/distance distribution was reasonably homogeneous. Excessive errors in P-wave onset readings were attempted avoided by waveform correlation between recording stations for each event subject to analysis. Also, for each event the network average residual was estimated and subtracted from the individual observations.

Travel time anomalies are caused by velocity variations within an a priori confined volume immediately beneath the station network (see Fig. VI.3.1), and thus are related to departures from standard earth models. The surface expression of this volume is marked in Fig. VI.3.2 and extends to a depth of 375 km. Also, the velocity structure is represented by a smooth cubic interpolatin between slowness values on a three-dimensional grid of 4x6x6 knots. This means that the upper mantle beneath the seismograph network is subdivided into 4 levels (0-75 km, 75-175 km, 175-275 km, 275-375 km) with slowness estimates at individual grids of 6x6 knots). Now the basis for linear inversion of travel time data is Fermat's principle stating that the variation in the travel time caused by small change in the ray path is zero to the first order. From this we may formulate a linearized relationship between travel time residuals (ΔT_{ij}) and velocity variations, namely:

$$\Delta T_{ij} = \int_{A_j}^{B_i} \delta s \, d\ell$$

where $s = 1/v$ is slowness or reciprocal velocity in s km^{-1}. A_j is the j-th receiver while B_i is the i-th source. This equation constitutes the very basis for linearized inversion of observed travel time residuals (the ACH-method and variants hereof) and for details here in this particular case, reference is made to Tryggvason (1981).

The validity of the linearity assumption above is based on the assumption that the non-linear terms are negligible, namely, the contributions due to change in velocity along the initial ray path and the effect of the change in ray path in the initial medium as detailed by Thomson and Gubbins (1981). We did indeed check the effects of these non-linear terms and found them ignorable.

Results

The anomaly maps of Figs. VI.3.2 represent the estimated P-wave fractional velocity anomalies for Iceland and adjacent areas. For details on the particular

'standard earth' model used, resolution and standard errors of the estimated velocity anomalies, etc., reference is made to Tryggvason (1981). It suffices to remark that for knots with resolution less than 0.4 and/or standard errors larger than the anomaly itself the corresponding knot fractional velocity estimates are not considered significant.

In layer 1 (Fig. VI.3.2a), which represents the uppermost 75 km, a broad and dominant low velocity zone is extending from the Tjörnes fracture zone (66.5°N, 16-19°W) north of Iceland, southward to the Krafla area (65.5°N, 17°W) and then west-southwestward in direction to the Snæfellsnes area (65°N, 19°W). This low coincides with a major part of the neovolcanic zone in northern and central Iceland together with late Quaternary and early Tertiary areas west of it. Pronounced low velocity values are tied to the Tjörnes shearing zone and the active Krafla volcanic area. Offshore there are only few significant anomalies and all of them represent a continuation of the pronounced high velocity regions in the southeastern and northwestern parts of the country. The grid points within Iceland itself are well resolved, that is, the resolution is around 80% and up to 90% in southern Iceland, which reflects a denser station network there. The standard error estimates for these most significant grid point values are around 1% relative velocity change. The capital letters A-A' and B-B' together with the heavy arrows indicate vertical cross-sections through the model box (Fig. VI.3.2).

In layer 2 (Fig. VI.3.2b), which ranges from 75 to 175 km depth, the low velocity zone is shifted southeastward compared to layer 1 and with the strongest anomalies south of Reykjanes (Keflavik), beneath the Hekla area (65°N, 16°W) and northeast of Kverkfjöll. A continuation of the high in the northwestern part of the country is obvious. In addition, two highs are prominent, namely, south of Iceland and northeast of Iceland. These areas are poorly sampled in layer 1, so a comparison between the two layers is not possible there.

For layer 3 (Fig. VI.3.2c), depth range 175-275 km, somewhat different features appear compared to the two uppermost layers. A significant low is covering an area south of the Tjörnes fracture zone and extending westward to the southwest

of the Kolbeinsey ridge. Another low velocity zone, but a weaker one, is underneath central and southwest Iceland. The resolution values are even higher here than in layer two, most of them around 0.9 and with accompanying standard errors down to 0.8%.

Layer 4 (Fig. VI.3.2d) covering the depth range of 275-375 km, is marked by a prominent velocity low beneath central Iceland. This is a relatively broad area with maximal east-west and north-south extension around 300 and 200 km respectively. The resolution and standard error estimates are about the same as for layer 3. For the lower layers most of the edge points are sufficiently well resolved. Significant anomaly contours can therefore be drawn quite to the edge of the box, as is the case for the highs around the country in layers 3 and 4.

We made two vertical cross-sections (Figs. VI.3.2) of the above four-layer anomaly patterns. The sections visualize the main lows and highs of all four layers, indicating an anomalous mantle beneath Iceland. Below circa 250 km depth of central Iceland a dominant low velocity zone might indicate a mantle plume or a so-called hot spot. Another strong low in the uppermost 70-80 km is beneath almost the whole of Iceland except for the periphery of the oldest rocks mainly in the SE and NW parts of the country. A broad 'transition zone' of relatively low velocities including a few strong low velocity pockets (see layers 2,3 of the anomaly maps) is clearly connecting the two major lows.

Discussion

To our knowledge, this is the very first time a comprehensive 3-D mapping of the Icelandic rift zone has been undertaken. Of particular interest is that the surface rift manifestations are reflected at depths of the order of 350 km as discussed by Tryggvason (1981). It is here tempting to draw a parallel to the NORSAR siting area which coincides with an ancient (Permian) aborted rift zone. Also here there are strong indications that the relatively large time and amplitude anomalies observed are caused by heterogeneities of

a predominantly vertical extent (e.g., see Christoffersson and Husebye, 1979; Haddon and Husebye, 1978; Thomson and Gubbins, 1982; and Troitskiy et al, 1981).

K. Tryggvason

E.S. Husebye

References

Aki, K., A. Christoffersson & E.S. Husebye, 1977: Determination of the three-dimensional seismic structure of the lithosphere, J. Geophys. Res., 82, 277-296.

Anderson, D.L., 1981: Hotspots, basalts and the evolution of the mantle. Science, 213, 82-89.

Christoffersson, A. & E.S. Husebye, 1979: On three-dimensional inversion of P wave time residuals: Option for geological modelling. J. Geophys. Res., 84, 6168-6176.

Gubbins, D., 1981: Source location in laterally varying media. In: Identification of Seismic Sources - Earthquake or Underground Explosion, eds. E.S. Husebye & S. Mykkeltveit, D. Reidel Publ. Co.

Haddon, R.A.W., & E.S. Husebye, 1978: Joint interpretation of P-wave time and amplitude anomalies in terms of lithospheric heterogeneities. Geophys. J.R. Astr. Soc., 55, 19-44.

Hovland, J., D. Gubbins & E.S. Husebye, 1981: Upper mantle heterogeneities beneath central Europe. Geophys. J.R. astr. Soc., 66, 261-284.

Thomson, C.J. & D. Gubbins, 1982: Three-dimensional lithospheric modelling at NORSAR: Linearity of the method and amplitude variations from the anomalies. Geophys. J.R. astr. Soc., in press.

Troitskiy, P., E.S. Husebye & A. Nikolaev, 1981: Earth holography experiment - lithospheric studies based on the principles of holography. Nature, 294, 618-623.

Tryggvason, K., 1981: 3-D mapping of the Iceland hot spot. NORSAR Tech. Rep. 4/81.

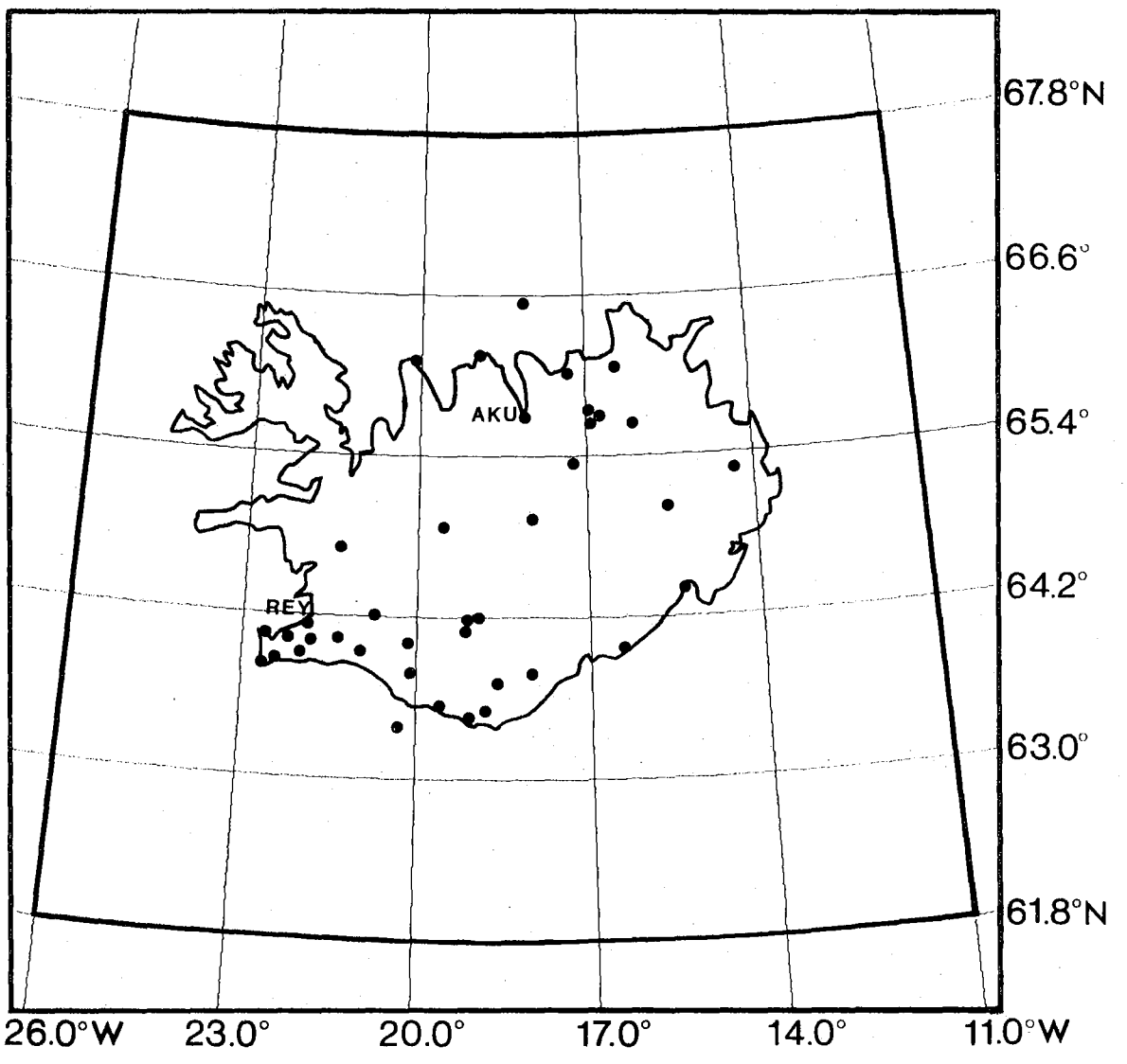

Fig. VI.3.1 The Icelandic seismograph network of 39 seismograph stations used in analysis. The model box is circumscribed with heavy lines. The latitude/longitude grid system intersections correspond to the model knots used in the time residual inversion as detailed in Tryggvason (1981).

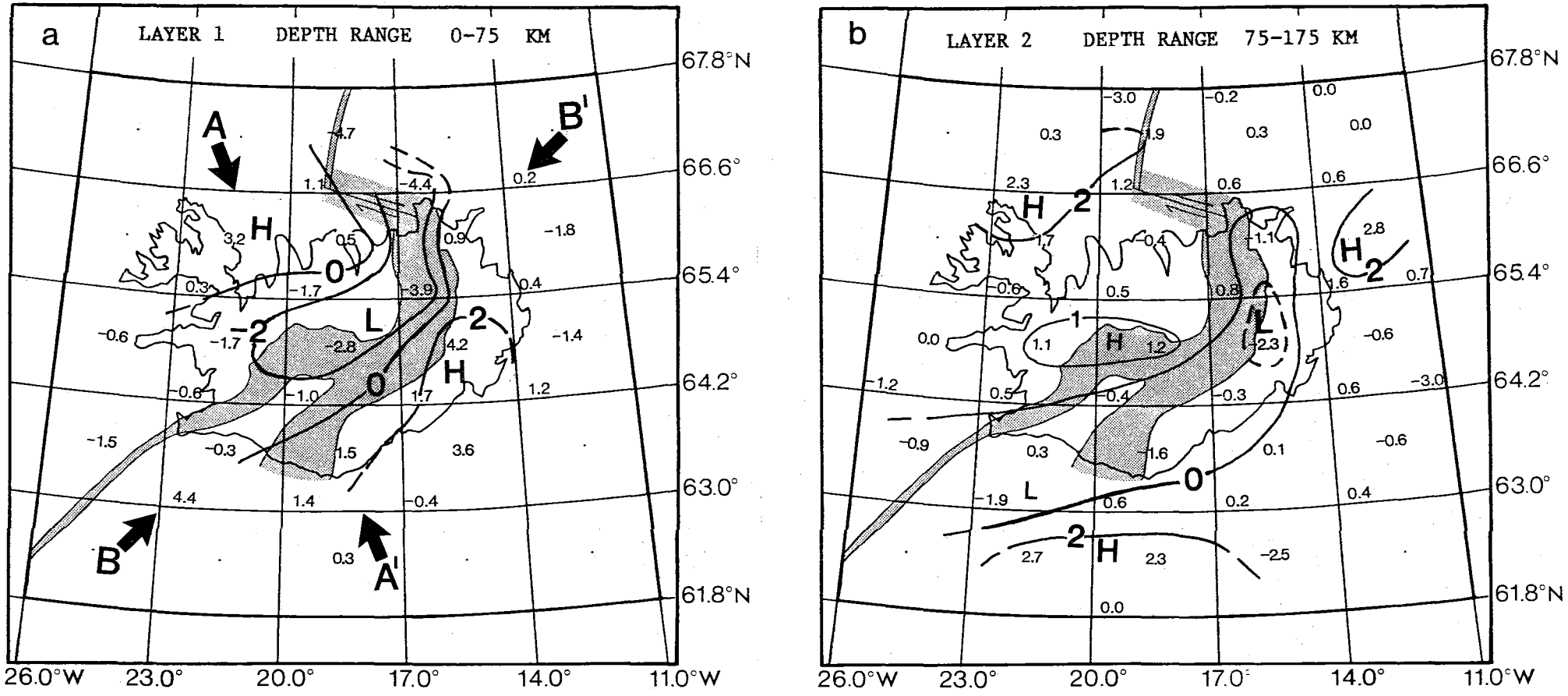

Fig. VI.3.2 (a) Velocity perturbations (in per cent) for layer 1. Areas of high and low velocities are indicated by capital letters H and L. The captial letters A-A' and B-B' together with the heavy arrows indicate vertical cross-sections through the model box as shown in Fig. VI.3.3. Resolution and standard errors for all knots are detailed in Tryggvason (1981). Figs. VI.3.1b,c & d captions as in (a) applied to the respective layers.

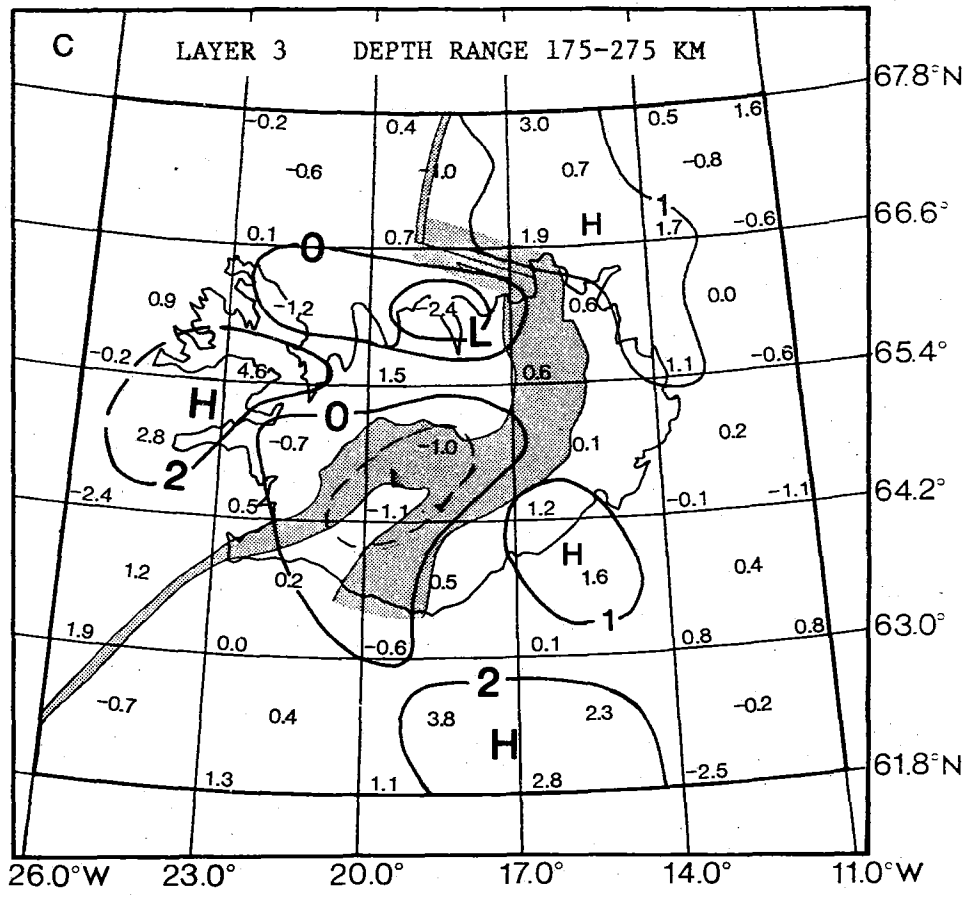

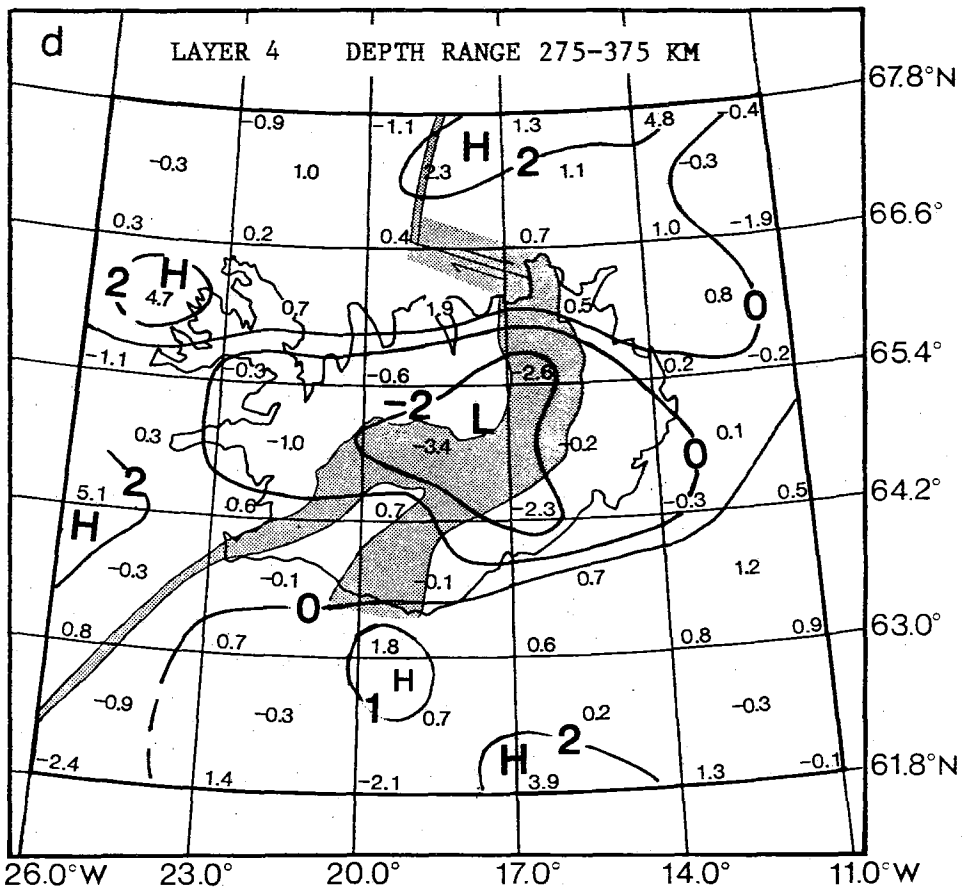

Fig. VI. 3.2 (continued).

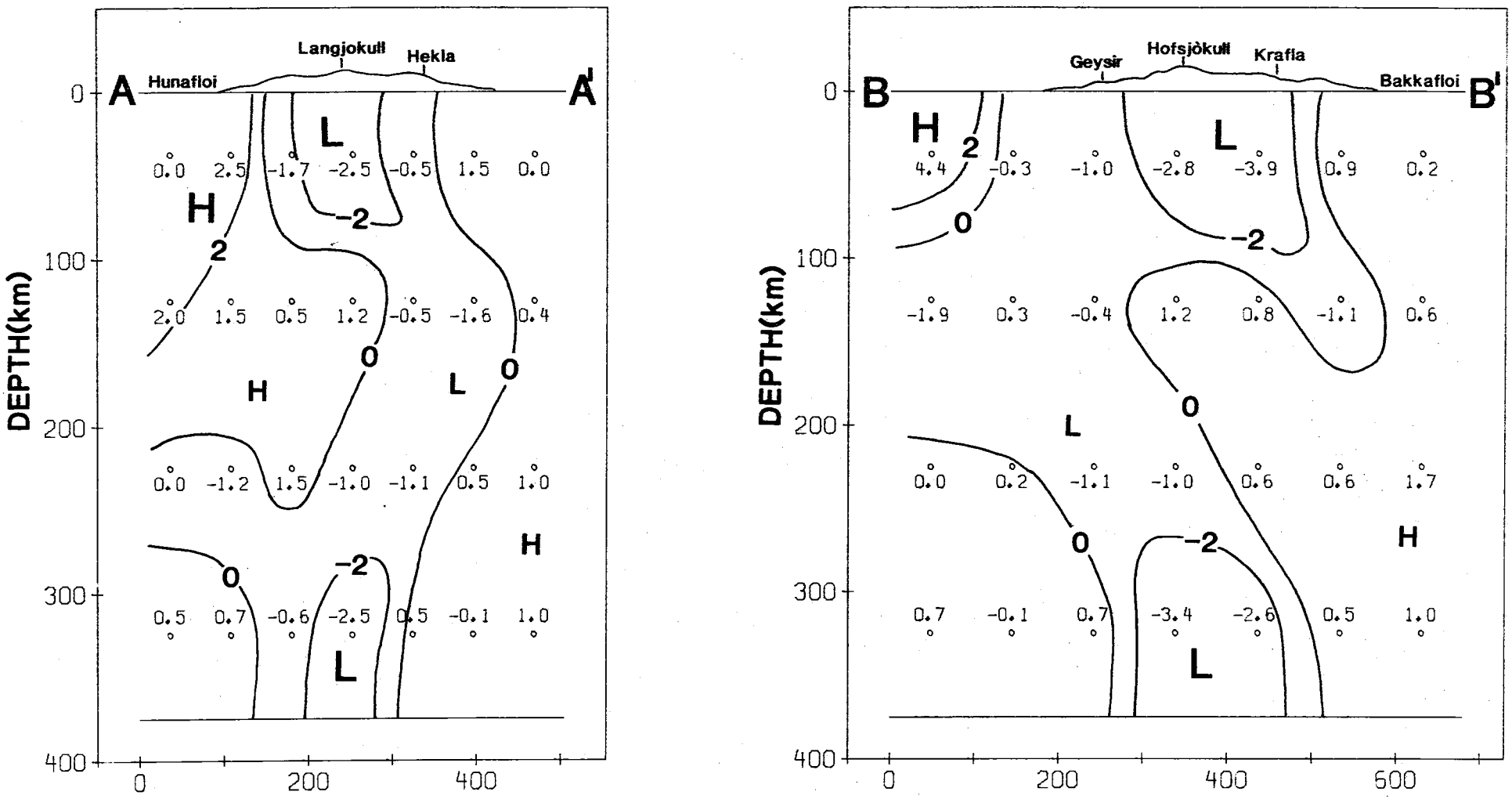

Fig. VI.3.3 The cross-sections span the latitude range from 63.°N to 66.0°N, from NW to SE (A-A') and from SW to NE (B-B'). The depth to distance scale is 2:1.

VI.4 Mantle heterogeneities beneath Fennoscandia

As part of NORSAR's comprehensive program for seismological mapping of upper mantle heterogeneities, travel time observations from the Fennoscandian network (Fig. VI.4.1) have been subjected to a 3-D inversion analysis similar to that described in Section VI.3. The region in question is interesting in the sense that the Baltic Shield constitutes its dominant tectonic feature as shown in Fig. VI.4.2. We note in passing that NORSAR scientists and colleagues in the past have undertaken detailed studies of parts of this region, e.g., see King and Calcagnile (1975), Aki et al (1977), England et al (1978), Haddon and Husebye (1978), Christoffersson and Husebye (1979), Calcagnile and Panza (1978), Sacks et al (1978), Troitskiy et al (1981) and Thomson and Gubbins (1982).

Data analysis and results

The observations in terms of P-wave travel time residuals were taken from the ISC bulletin tapes for the period 1964-77 and thus permitted us to include stations no longer operational like KRK, GOT & KLS (Fig. VI.4.1). The motivation for this was that the minimum size of structural heterogeneities to be resolved is a function of the station interspacing within the network. In this respect the Fennoscandian network is much coarser than that of Iceland (Section VI.3) and not at all comparable to that of NORSAR itself (Troitskiy et al, 1981). At a later stage, however, we will use data from the new, southern Scandinavian network, which comprises some 25 new stations with an interspacing of around 50-75 km.

The Fennoscandian inversion results in terms of percentage seismic velocity anomalies are displayed in Fig. VI.4.2. The standard earth reference model used was that of Dziewonski et al (1975) for continental areas. The estimated standard errors were of the order of 1 per cent except for poorly resolved (resolution less than 0.5) peripheral nodes which are specially marked in Fig. VI.4.2. In the following we will comment on the velocity anomaly patterns at the respective levels.

Level 1 (0-100 km). The anomaly pattern here is dominated by a velocity high over the central parts of Fennoscandia, the Bothnian Bay. Otherwise, there is indication of a negative anomaly straddling the Barents Sea to the northwest. This is an intracontinental sedimentary basin whose crustal structure is found to be considerably different from that of the Baltic Shield (e.g., see Levshin and Berteussen, 1978; and Bungum et al, 1981). Unfortunately, the resolution was very poor in the southern part of the network area, so it was not feasible to test whether the various tectonic provinces adjacent to the Baltic Shield (Fig. VI.4.x) also have a seismic manifestation.

Level 2 (100-300 km). The anomaly pattern here is rather similar to that of level 1 with velocity lows in the Caledonides of western and northern Norway. The dominant velocity high coincides roughly with the areal extent of the Baltic Shield and thus confirms long-standing hypotheses that such tectonic provinces constitute deep-seated, relatively homogeneous parts of the upper mantle in analogy with the tectonosphere concept.

Level 3 (300-500 km). The characteristic features here are weak anomalies and no similarity to those at level 2. In a plate tectonic context we may take levels 1 and 2 to constitute the lithosphere which in turn is decoupled from the underlying asthenosphere of level 3. Sacks et al (1978) reported indications of a discontinuity beneath the Bothnian Bay at a depth of 230 km which tentatively has been interpreted as the lithosphere/asthenosphere boundary. Likewise, Calcagnile (1982) on the basis of Rayleigh wave dispersion analysis finds that the central parts of the Baltic Shield exhibit a considerably thicker lithosphere than the adjacent areas to the west.

Level 4 (500-600 km). Also this layer appears remarkably homogeneous, although less so than layer 3. The very existence of heterogeneities in this part of the upper mantle is probably related to geochemical/geothermal anomalies associated with the 650 km discontinuity. We remark that heterogeneities at depths greater than 600 km may be 'projected' into layer 4.

Discussion

The essential result obtained is that the surface expression of the Baltic Shield has a relatively high seismic velocity counterpart some 300 km down in the upper mantle. Quantitatively, this explains some characteristic features of Fennoscandian seismograph recordings, namely, relatively large amplitude P-wave recordings and 'early' arrival times for events in western Russia and central Asia. In a future study we will attempt to quantify wave propagation through 3-D media of the above kind also in terms of an associated Q-structure.

E.S. Husebye

J. Hovland

References

Aki, K., A. Christoffersson & E.S. Husebye, 1977: Determination of the three-dimensional seismic structure of the lithosphere, J. Geophys. Res., 82, 277-296.

Bungum, H., S.E. Pirhonen & E.S. Husebye, 1980: Crustal thicknesses in Fennoscandia. Geophys. J.R. astr. Soc., 63, 759-774.

Calcagnile, G., 1982: The lithosphere-asthenosphere system in northwestern Europe inferred from the dispersion of surface waves. Tectonophysics, in press.

Calcagnile, G. & G. F. Panza, 1978: Crust and upper mantle structure under the Baltic Shield and Barents Sea from the dispersion of Rayleigh waves. Tectonophysics, 47, 59-71.

Christoffersson, A. & E.S. Husebye, 1979: On 3-dimensional inversion of P-wave time residuals. Option for geological modeling. J. Geophys. Res., 84, 6168-6176.

Dziewonski, A.M., H.L. Hales & E.R. Lapwood, 1975: Parametrically simple earth models consistent with geophysical data. Phys. Earth Planet. Int., 10, 12-48.

England, P.C., B.L.N. Kennett & M.H. Worthington, 1978: A comparison of the upper mantle structure beneath Eurasia and the North Atlantic and Arctic Oceans, Geophys. J.R. astr. Soc., 54, 575-585.

Haddon, R.A.W. & E.S. Husebye, 1978: Joint interpretation of P-wave time and amplitude anomalies in terms of lithospheric heterogeneities. Geophys. J.R. astr. Soc., 55, 19-44.

Hovland, J. & E.S. Husebye, 1981: Three-dimensional seismic veloccity image of the upper mantle beneath southeastern Europe. In E.S. Husebye & S. Mykkeltveit (eds.), Identification of Seismic Sources - Earthquake or Underground Explosion, 589-605, D. Reidel Publ. Co.

Hovland, J., D. Gubbins & E.S. Husebye, 1981: Upper mantle heterogeneities beneath central Europe. Geophys. J.R. astr. Soc., 66, 261-284.

King, D.W. & G. Calcagnile, 1976: P-wave velocities in the upper mantle beneath Fennoscandia and western Russia, Geophys. J.R. astr. Soc., 46, 407.

Levshin, A. & K.-A. Berteussen, 1979: Anomalous propagation of surface waves in the Barents Sea as inferred from NORSAR recordings. Geophys. J.R. astr. Soc., 56, 97-118.

Sacks, I.S., J.A. Snoke & E.S. Husebye, 1979: Lithosphere thickness beneath the Baltic Shield. Tectonophysics, 56, 101-110.

Thomson, C. & D. Gubbins, 1982: Three-dimensional lithospheric modelling at NORSAR: Linearity of the method and amplitude variations from the anomalies. Geophys. J.R. astr. Soc., in press.

Troitskiy, P., E.S. Husebye & A. Nikolaev, 1981: Lithospheric studies based on holographic principles. Nature, 294, 618-623.

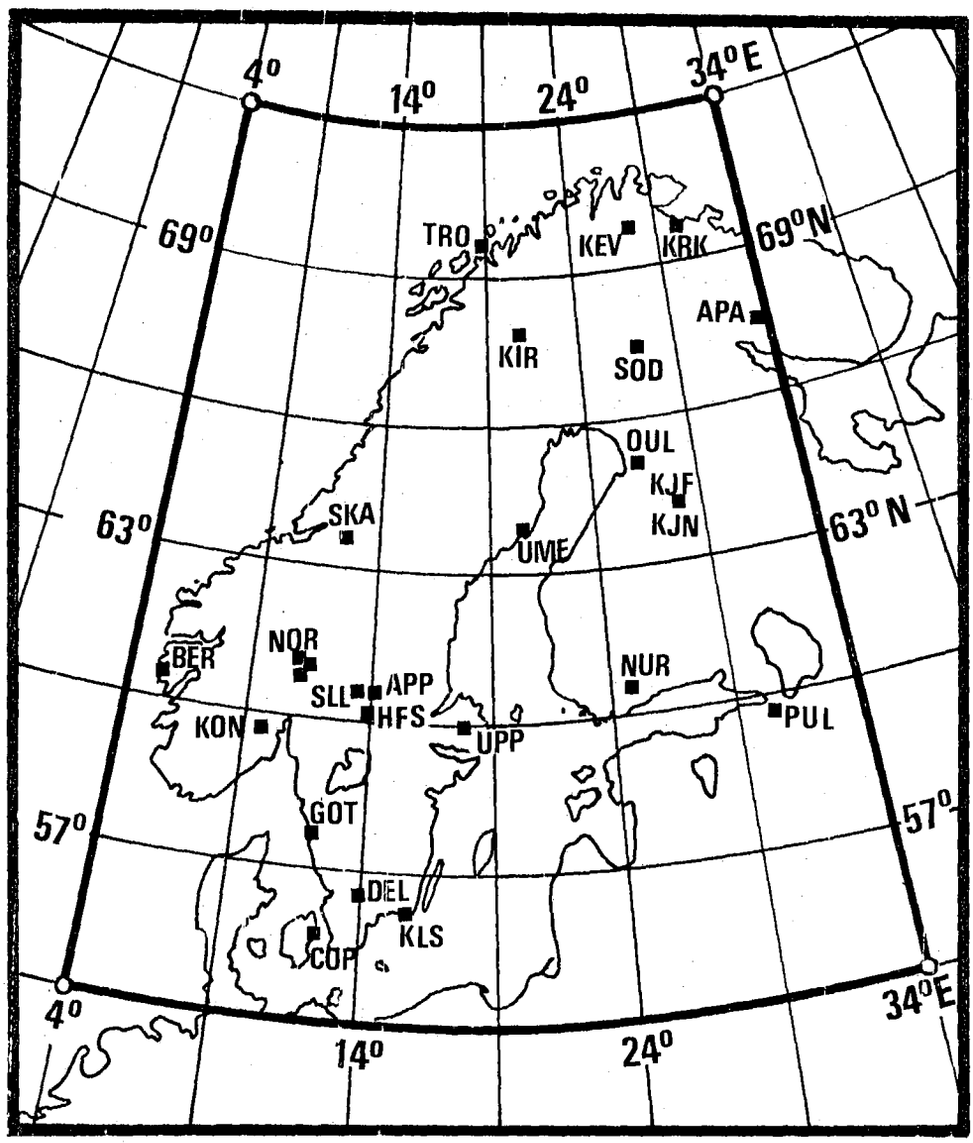

Fig. VI.4.1 Fennoscandian seismograph network whose P-wave travel time residual reportings to ISC were used in analysis.

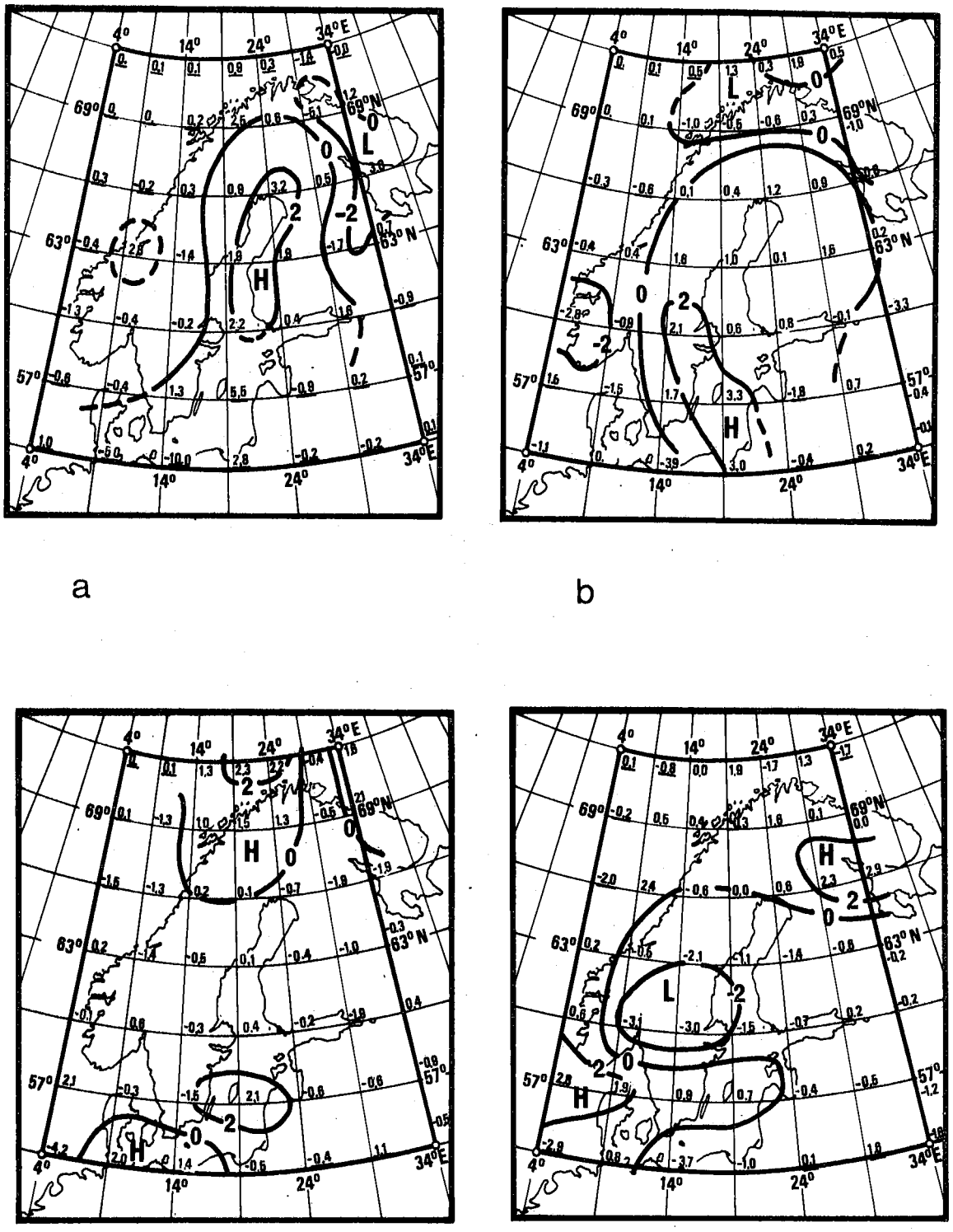

Fig. VI.4.2 (a) Velocity perturbations in per cent for Level 1 (0-100 km). Areas of high and low velocities are indicated by captial letters H and L. (b) Velocity perturbations in per cent for Level 2 (100-300 km). (c) Velocity perturbations in per cent for Level 3 (300-500 km). (d) Velocity perturbations in per cent for Level 4 (500-600 km).

VI.5 Upper mantle heterogeneities beneath Eastern Europe

Travel time residuals for east European seismograph stations (see Fig. VI.5.1) as reported to the ISC have been used in a study of upper mantle heterogeneities beneath eastern Europe. Standard 3-D inversion procedures were used in the data analysis and the results obtained are displayed in Fig. VI.5.2. In the next section these results will be discussed in some detail, and also a comparison will be made with similar results reported for central Europe (Hovland et al, 1981) and Greece and adjacent areas (Hovland and Husebye, 1981).

3-D inversion results for eastern Europe

The east European inversion results in terms of percentage seismic velocity anomalies are displayed Fig. VI.5.2. The standard earth reference model used was that of Dziewonski et al (1975) for continental regions. The estimated standard errors were of the order of 0.6 per cent except for poorly resolved peripheral nodes (resolution less than 0.5). For details see Table VI.5.1. In the following we will comment on the velocity anomaly patterns at the respective levels.

Level 1 (0-100 km). The anomaly pattern is dominated by velocity lows over the Pannonian Basin and western Turkey, both of which are characterized by high heat flows. Most of the peripheral nodes are poorly resolved but in this respect the velocity high near the northwest corner is exceptional. From its estimated resolution (0.7) and standard error (0.7 per cent) this node should be rated significant, but its estimated bias error (Thomson and Gubbins, 1982) is of the order of 3 per cent.

Level 2 (100-300 km). The areas of velocity lows are even more dominant at this level, and there is a certain overlap with level 1 results for the Pannonian Basin and the western Turkey/Aegean Sea. The velocity highs are found towards west and north. An axiom of modern plate tectonic hypothesis is a lithosphere/asthenosphere decoupling which in this particular case should imply rather pronounced anomaly pattern differences between the level 1 and 2 results. This clearly does not apply to areas of pronounced velocity lows like the Pannonian Basin and the Aegean Sea. However, both of these areas are hypothesized to be associated with upwelling asthenospheric material

(for discussion here, see Hovland and Husebye, 1981) and thus a level 1/2 coupling is indeed expected for these two areas.

Level 3 (300-500 km). Relative to level 2 the anomaly pattern here changes rather abruptly with a pronounced velocity high now in the Aegean Sea, while areas of velocity lows are of rather modest extents.

Level 4 (500-600 km). The anomaly pattern of level 3 is essentially retained here with relatively pronounced anomalies in comparison to those observed for Fennoscandia for these two levels.

Discussion

The station distribution within the eastern European seismograph network (as defined in Fig. VI.5.1) is skew in the sense that most stations are found in the NW and SE quandrants. This in turn is reflected in relatively poorly resolved nodes in the NE and SW quadrants as demonstrated in Table VI.5.1. Notwithstanding this kind of problems, the stable tectonic units of the region under investigation, namely, the Ukranian Shield and the East European Platform, correspond to those areas which exhibit modest velocity anomalies at the four levels of Fig. VI.5.2.

The eastern European region as defined in Fig. VI.5.x overlaps partly with that of Central Europe (Hovland et al, 1981) and southeast Europe (Hovland and Husebye, 1981). Although different data sets are used, the anomaly patterns of the various studies correlate well in the overlapping areas (not unexpected).

An intriguing aspect of the results presented is the existence also in the asthenosphere of strong velocity anomalies. This feature is less pronounced for platform and shield areas, which exhibit relatively very good P-wave propagation regimes in terms of early phase arrivals with relatively strong high-frequency signal amplitudes. This and associated topics of 3-D

seismic modelling of the lithosphere/asthenosphere will be the subject of future NORSAR research studies.

J. Hovland

E.S. Husebye

References

Dziewonski, A.M., H.L. Hales & E.R. Lapwood, 1975: Parametrically simple earth models consistent with geophysical data. Phys. Earth Planet. Int., 10, 12-48.

Hovland, J. & E.S. Husebye, 1981: Three-dimensional seismic veloccity image of the upper mantle beneath southeastern Europe. In E.S. Husebye & S. Mykkeltveit (eds.), Identification of Seismic Sources - Earthquake or Underground Explosion, 589-605, D. Reidel Publ. Co.

Hovland, J., D. Gubbins & E.S. Husebye, 1981: Upper mantle heterogeneities beneath central Europe. Geophys. J.R. astr. Soc., 66, 261-284.

Thomson, C. & D. Gubbins, 1982: Three-dimensional lithospheric modelling at NORSAR: Linearity of the method and amplitude variations from the anomalies. Geophys. J.R. astr. Soc., in press.

RESOLUTION								STANDARD ERROR						
							LEVEL 1							
0.3	0.7	0.2	0.3	0.1	0.0	0.0		0.8	0.7	0.6	0.7	0.4	0.1	0.1
0.7	0.7	0.6	0.7	0.6	0.1	0.0		0.7	0.6	0.7	0.6	0.6	0.3	0.1
0.4	0.5	0.6	0.5	0.4	0.5	0.0		0.8	0.7	0.7	0.7	0.7	0.6	0.1
0.0	0.2	0.2	0.5	0.5	0.5	0.0		0.2	0.6	0.6	0.7	0.7	0.7	0.2
0.0	0.4	0.2	0.6	0.6	0.5	0.6		0.2	0.5	0.6	0.6	0.7	0.7	0.7
0.0	0.0	0.0	0.6	0.5	0.5	0.3		0.1	0.1	0.2	0.6	0.5	0.6	0.7
0.0	0.0	0.0	0.1	0.1	0.0	0.0		0.0	0.0	0.1	0.5	0.4	0.1	0.1
							LEVEL 2							
0.6	0.8	0.7	0.6	0.4	0.1	0.0		0.8	0.6	0.7	0.7	0.7	0.4	0.1
0.8	0.8	0.8	0.7	0.7	0.5	0.0		0.7	0.5	0.5	0.5	0.5	0.6	0.3
0.6	0.7	0.7	0.7	0.7	0.6	0.3		0.7	0.5	0.5	0.5	0.6	0.4	0.8
0.2	0.6	0.6	0.6	0.7	0.7	0.2		0.7	0.6	0.6	0.5	0.5	0.5	0.7
0.5	0.6	0.5	0.7	0.7	0.7	0.8		0.7	0.4	0.7	0.5	0.5	0.5	0.6
0.0	0.1	0.3	0.6	0.7	0.6	0.6		0.3	0.4	0.6	0.4	0.5	0.5	0.7
0.0	0.0	0.0	0.4	0.5	0.1	0.0		0.0	0.0	0.3	0.8	0.7	0.5	0.3
							LEVEL 3							
0.6	0.8	0.8	0.7	0.7	0.5	0.0		0.8	0.6	0.6	0.7	0.7	0.7	0.4
0.8	0.8	0.8	0.8	0.8	0.7	0.3		0.7	0.5	0.4	0.4	0.5	0.5	0.7
0.6	0.8	0.8	0.8	0.7	0.7	0.6		0.7	0.5	0.5	0.5	0.5	0.5	0.8
0.5	0.7	0.7	0.7	0.7	0.7	0.6		0.8	0.5	0.5	0.5	0.5	0.5	0.8
0.4	0.5	0.7	0.7	0.8	0.7	0.7		0.8	0.7	0.5	0.5	0.4	0.5	0.7
0.2	0.4	0.6	0.7	0.7	0.7	0.6		0.8	0.8	0.5	0.5	0.5	0.5	0.8
0.0	0.0	0.3	0.5	0.6	0.5	0.1		0.1	0.1	0.8	0.8	0.8	0.8	0.6
							LEVEL 4							
0.2	0.4	0.5	0.5	0.3	0.3	0.0		0.6	0.8	0.8	0.8	0.8	0.8	0.3
0.3	0.5	0.6	0.6	0.5	0.4	0.2		0.8	0.8	0.7	0.7	0.7	0.7	0.6
0.4	0.4	0.5	0.6	0.5	0.4	0.3		0.8	0.7	0.7	0.7	0.7	0.7	0.7
0.2	0.4	0.5	0.5	0.5	0.5	0.4		0.7	0.7	0.7	0.7	0.7	0.7	0.8
0.1	0.2	0.4	0.4	0.5	0.5	0.4		0.5	0.6	0.7	0.7	0.7	0.7	0.8
0.0	0.2	0.3	0.3	0.4	0.4	0.3		0.3	0.6	0.7	0.7	0.7	0.8	0.8
0.0	0.0	0.1	0.1	0.2	0.2	0.1		0.1	0.2	0.5	0.7	0.7	0.7	0.5

TABLE VI.5.1

Resolution and standard errors for the individual knot estimate of velocity perturbations shown in Fig. VI.5.2.

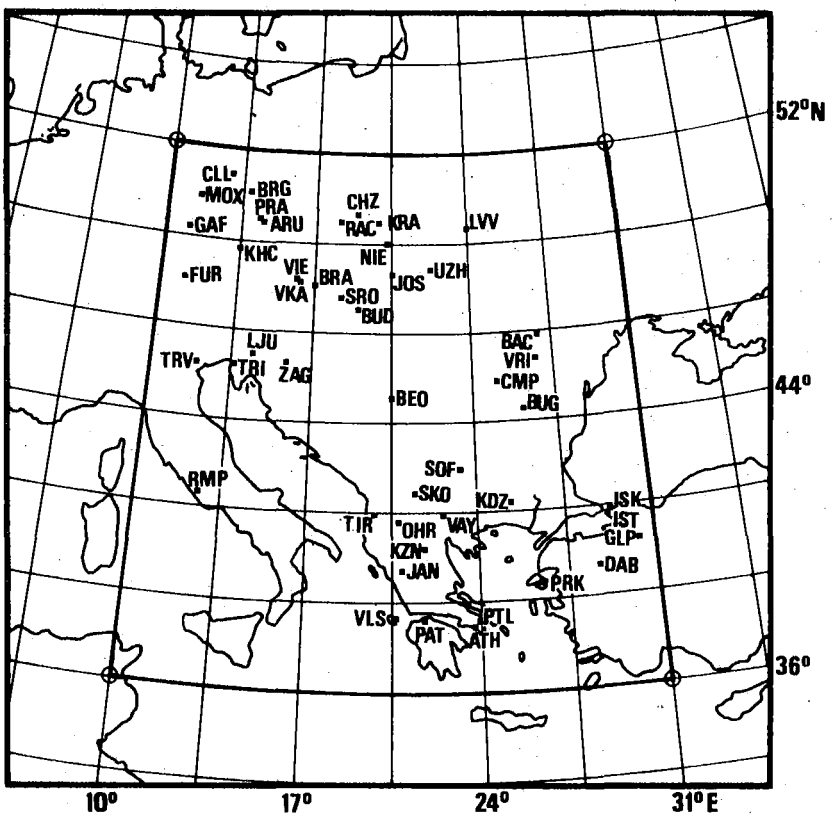

Fig. VI.5.1 The eastern Europe seismograph station network used in analysis. The intersections of the latitude/longitude grid system correspond to the knots in the time residual inversion results shown in Fig. VI.5.2.

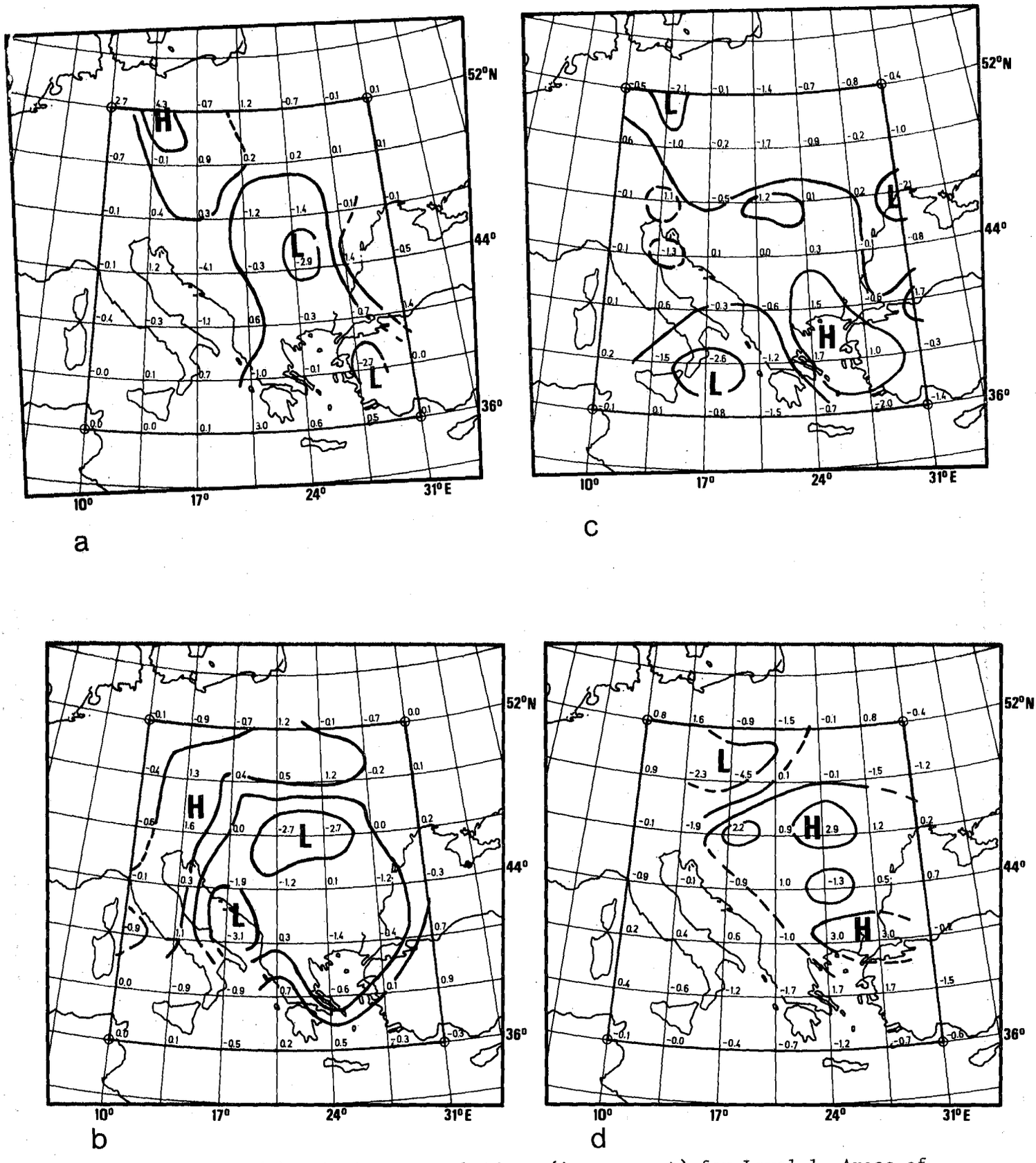

Fig. VI.5.2 (a) Velocity perturbations (in per cent) for Level 1. Areas of high and low velocities are indicated by capital letters H and L. Resolution and standard errors for all knots are listed in Table VI.5.1. (b) Velocity perturbations (in per cent) for Level 2. (c) Velocity perturbations (in per cent) for Level 3. (d) Velocity perturbations (in per cent) for Level 4.

VI.6 Signal detection using P-wave envelope representation

The beamforming technique conventionally used for detection processing at seismic arrays such as NORSAR is critically dependent upon signal coherency across the array for good performance. Earlier studies, e.g., Ringdal et al (1975) have shown that in numerous instances, particularly for regional events and events with high dominant signal frequency, signal coherency is generally poor across the NORSAR array. A so-called 'incoherent' beamforming detector, which essentially sums the envelopes of the filtered sensor traces, has shown superior performance compared to standard beamforming in such cases, and such a detector has in fact been in operation at NORSAR since 1971.

A study has been undertaken (Nysæter, 1981) to analyze in detail the performance of envelope detectors on NORSAR data, both as a function of envelope representation technique and filter setting. Two representation techniques have been investigated:

(a) Using a sliding short term rectified average (STA), based on a window of 1.5 seconds of the filtered signal of each trace;
(b) Using a squared Hilbert transform of the filtered signal of each trace.

An illustration of these envelope representations is given in Fig. VI.6.1. The Hilbert transform provides a theoretical envelope to the signal, whereas the STA representation is only approximate. On the other hand, the STA envelope is faster to compute.

The actual detection algorithm for each of the two representations has consisted of

(i) Prefiltering of each of 7 sensor traces (one per subarray) with a recursive Butterworth bandpass filter
(ii) Computing the appropriate envelope of each trace
(iii) Summing the envelopes with 64 sets of time delays (as in the NORSAR on-line system)
(iv) Applying a standard linear STA/LTA detector.

The subsequent analysis steps were as follows:

1. Evaluate the false alarm rate as a function of SNR by analyzing selected noise segments using both detectors.
2. Determine comparable thresholds for each detector (i.e., set a threshold such that the number of false alarms were similar).
3. Compare the signal-to-noise ratio of each of a set of 123 events for the two detectors, adjusted for the threshold differences.

The 123 events were based upon reportings from the full 42 element NORSAR SP array. With a false alarm rate comparable to that of the NORSAR on-line envelope detector, 115 and 112 of these events were detected by the Hilbert and STA envelope detectors, respectively. (Note that these detectors were based on 7 SP channels only.) Average SNR (adjusted for threshold differences) were 14.43 and 14.24 dB respectively, thus giving a very marginal improvement for the Hilbert algorithm relative to STA envelopes (see Fig. VI.6.2). This is in some contrast to the results by Wen-Wu-Chen (1974), who reported a significant improvement using Hilbert transforms relative to STA envelopes.

The effect of filter setting was investigated using a subset of 22 events, and applying filters of 2.0-4.0 Hz, 2.4-4.4 Hz and 2.8-4.8 Hz in addition to the standard 1.6-3.6 Hz filter used by the NORSAR on-line envelope beam detector. The results are summarized in Table VI.6.1, which shows that the filter band 2.0-4.0 Hz is the best overall, both with respect to the number of detections and the average SNR. Again, the difference between the two detectors is slight.

In summary, we have thus found:

1. An envelope beam detector based on the Hilbert transform is only slightly better than the computationally simpler envelope detector based on a sliding STA window.

2. A filter setting of 2.0-4.0 Hz appears to be near the optimum choice for overall detection of regional events, although individual variations in signal frequency may cause other bands to be better in some cases.

3. The performance of a 7 element array (one instrument from each subarray) is almost equal to that of the 42 element NORSAR array for regional events. This shows that event gains at the subarray beam level are quite modest for conventional beamforming of regional signals recorded at NORSAR.

A. Nysæter

References

Chen, W.W., 1974: Comparison of coherent and incoherent beamforming envelope detectors for NORSAR regional seismic events. Tech. Rep. No. 6, Texas Instruments Report No. ALEX(01)-TR-74-06, AFTAC Contract No. F08606-74-C-0033, Texas Instruments, Dallas, Texas.

Nysæter, A., 1981: Quadratic versus linear envelope beamforming for seismic event detection, NORSAR Tech. Report 3/81, NTNF/NORSAR, Kjeller, Norway.

Ringdal, F., E.S. Husebye & A. Dahle, 1975: P-wave envelope representation in event detection using array data. Proc. NATO ASI Exploitation of Seismograph Networks, Series E, 11, Nordhoff-Leiden, 353-372.

Frequency	1.6-3.6 Hz		2.0-4.0 Hz		2.4-4.4 Hz		2.8-4.8 Hz	
Bands	S-E	STA	S-E	STA	S-E	STA	S-E	STA
No. of detected events	19	19	22	22	19	16	17	16
Average SNR	19.13	18.58	20.90	20.14	20.78	19.69	19.70	18.45
SNR difference	0.55		0.76		1.09		1.25	

Table VI.6.1

Comparison of detection performance of 22 regional events reported by NORSAR for two envelope detectors: Square envelope Hilbert transform (S-E) and sliding STA window envelopes (STA).

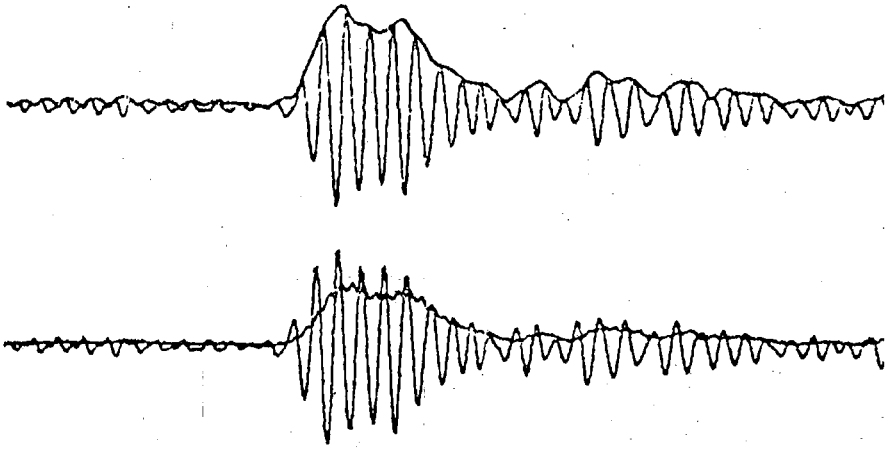

Fig. VI.6.1 Hilbert type envelope (top) and STA type envelope (bottom) of a seismic signal.

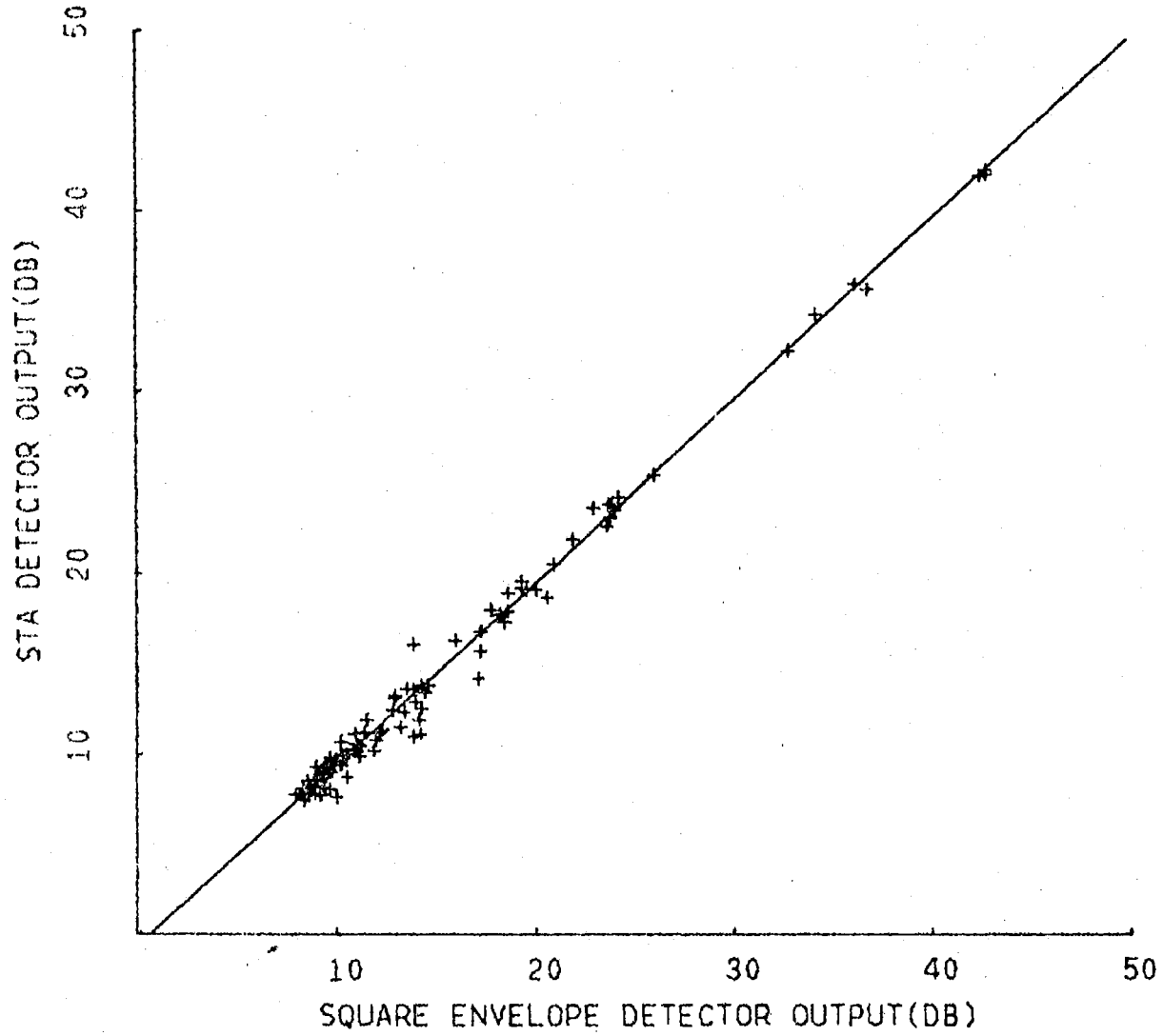

Fig. VI.6.2 Max. SNR from the square envelope detector versus max. SNR from the STA-detector for signals detected by both. The equation for the straight line is $y = -0.6 + x$, which corresponds to equal false alarm rate from the two detectors.

VI.7 Investigation of signal focusing effects at NORSAR for events near the Caspian Sea

A major feature of seismic signals recorded at the NORSAR array is the large amplitude variations seen between individual instruments for any given event (Berteussen and Husebye, 1974). The amplitudes typically differ by about a factor of 10 between the 'best' and 'worst' instrument, corresponding to about 1.0 m_b unit variation across the 100 km NORSAR aperture. The amplitude patterns are repeatable for any given source regions, but may change considerably with only a few hundred kilometers shift in epicenter. Thus, any one of the 22 original NORSAR subarrays is the 'best' one for at least one source region, and the 'worst' one for at least one other region.

For the Caspian Sea region, subarray 02B has the highest signal amplitudes. Even within this subarray, which has an aperture of only 10 km, there is a considerable variability in amplitudes, as seen in Fig. VI.7.1 for an event near Azgir, USSR. A project has been undertaken to investigate these signal focusing effects in more detail, using an experimental set of six sensors deployed near the instrument 02B05, which has the highest amplitudes for this source area (Fig. VI.7.2). The aims of this deployment are the following:

- Take advantage of the focusing effects to improve event detectability for this region
- Investigate signal spectra at high frequencies (the data will be sampled at 40 Hz with an analog cutoff filter at 12.5 Hz, thus giving improved spectral recordings at high frequencies compared to standard NORSAR SP channels)
- Monitor low magnitude earthquake activity in the Caspian Sea area.

The experimental array is expected to become operational early 1982.

F. Ringdal
P.W. Larsen

Reference

Berteussen, K.-A. & E.S. Husebye, 1974: Amplitude pattern effects on NORSAR P-wave detectability. NORSAR Sci. Rep. No. 1-74/75, NTNF/NORSAR, Kjeller, Norway.

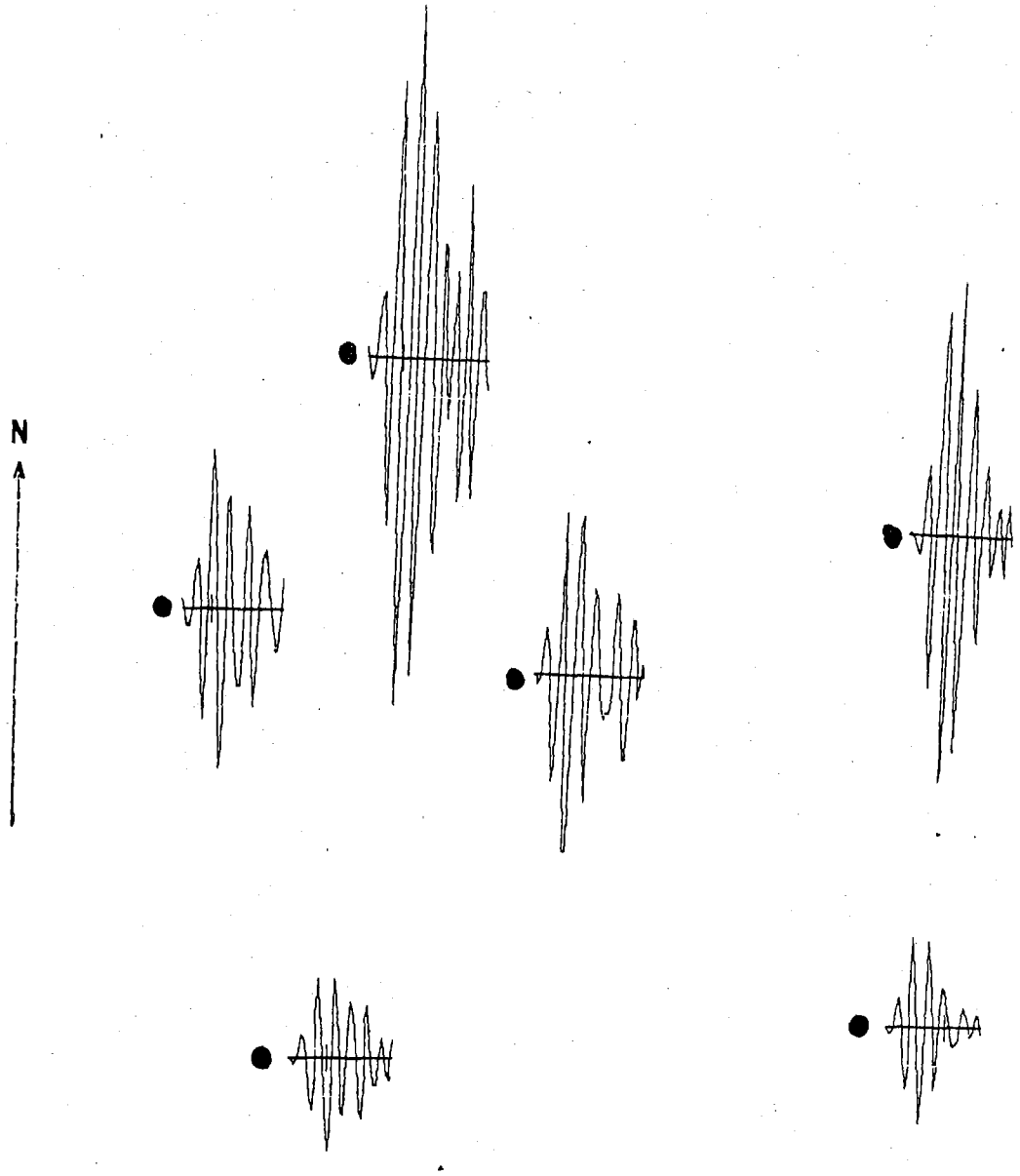

Fig. VI.7.1 Illustration of the amplitude variability within NORSAR subarray 02B for the P phase from an event near Azgir, USSR, Oct 14, 1977. The traces have been filtered with a 2.4-4.4 Hz bandpass filter, and the dots represent the positions of the 6 SP instruments in the subarray. (Subarray diameter is about 10 km.) There is a general trend of increasing amplitudes from south to north, with the amplitude at the northernmost instrument (02B05) being larger by a factor of 4 compared to the instruments furthest south.

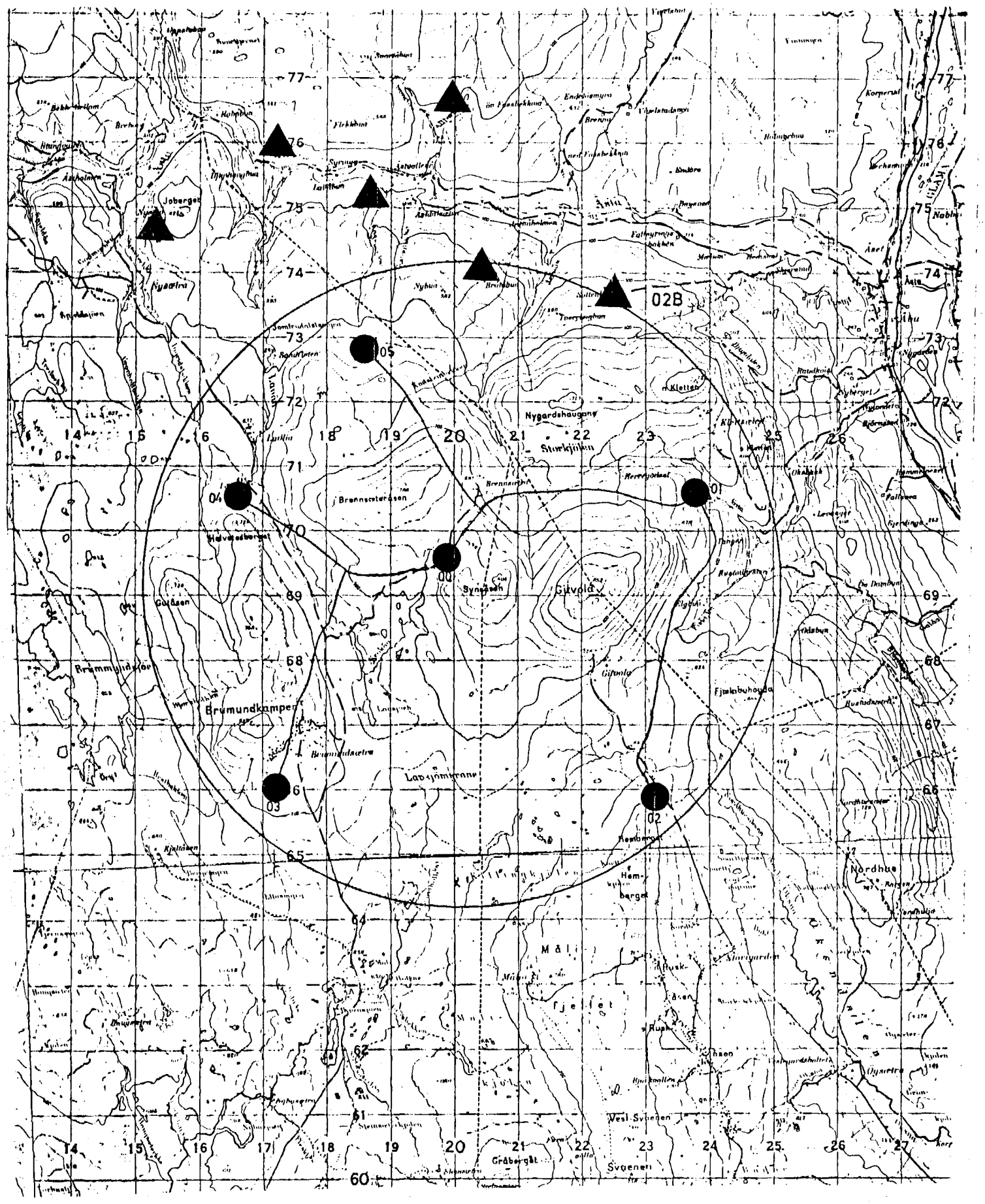

Fig. VI.7.2 NORSAR subarray 02B. Circles denote current NORSAR SP instruments, while triangles show the locations of six planned experimental SP sensors.

VI.8 Dynamic ray-tracing in complex three-dimensional models

In the last years, 3-D seismic modelling has become a rapidly growing branch of modern geophysical research. Within this area a very important tool is the seismic ray-tracing methods, which have recently been extended to include even dynamic properties of the wave field.

We have developed a rather general 3-D ray-tracing system suitable for application to various kinds of seismic modelling problems. (For details see Gjøystdal, 1978A,B; Gjøystdal, 1979; Gjøystdal & Ursin, 1981; Gjøystdal et al, 1981; Reinhardsen, 1981.)

One of the major problems considered is how to represent a 3-D geological model mathematically. The various seismic reflectors are divided into a system of bicubic spline surfaces. A special kind of 'logic' has been developed in order to obtain a proper connection between the various spline interfaces, permitting an unambiguous tracing of any ray through the model, provided the ray has specified direction in the start point. The layers between the interfaces may have any velocity variation, provided the velocity function is continuous and has continuous 1st and 2nd derivatives everywhere in each layer.

Particularly in the last 5 years there have been a number of works on the problem of extending the ray-tracing procedures to include parameters in addition to those just mentioned. For example, Hubral and Krey have published several papers on wavefront curvature calculations, and last year Cerveny and Hron presented an excellent theoretical work on the ray series method and dynamic ray-tracing in 3-D inhomogeneous media. (For reference, see f.ex. Hubral and Krey, 1980; and Cerveny and Hron, 1980.) We have included these methods in a 3-D ray-tracing system. A new dimension is introduced into such a dynamic ray-tracing system in that we are now able to calculate wavefront curvatures and amplitudes at any point of a ray (see Fig. VI.8.1). The 'dynamic' procedures are able to make proper use of the parameters of the medium sampled by the ray, such as velocity gradients, interface curvatures, etc., which were just ignored in 'conventional' ray-tracing.

In mathematical terms, the wavefront is represented by a 2 by 2 wavefront curvature matrix, which essentially contains the wavefront curvatures in two principal directions perpendicular to each other. There now exist theoretical procedures for calculation of the change in the wavefront curvature matrix on refraction or reflection at an interface. In order to calculate the change in the wavefront curvature matrix and amplitude coefficients when tracing the ray through a continuous part of the medium, we have to solve a set of differential equations. These are non-linear equations that must generally be solved by numerical approximations. For general velocity media, we have used the so-called Admas P-E-C-E method in order to solve the equations (Predict-Evaluate-Correct-Evaluate). For media with constant velocity or constant velocity gradient, we can obtain analytical solutions of the equations, of course making the process considerably more efficient.

We have developed a special search procedure in order to find ray paths connecting a given source- and receiver-position in a 3-D model. It is based on the 'shooting method', that is, we are starting in the shot point with a certain initial direction of the ray, and the ray is traced through the model until a specified 'receiver interface' has been reached. The initial ray direction is then updated and a second ray is traced through the model. The procedure is then repeated until the ray arrives sufficiently close to the specified receiver point. The procedure is described in detail in Gjøystdal (1978A,B); here we shall restrict ourselves to stating some basic properties of the method. The procedure takes advantage of a 'receiver line' running through the receiver point. The search constitutes a 'curve crawling process' along this line, using gradient calculations for updating the ray direction at each iteration step. The procedure is especially efficient when a number of receivers are distributed along a line (or continuous curve), as is usually the case in geophysical exploration. In addition, the procedure is designed to pick up the various branches of the travel time function if such branches exist, thus being able to determine all ray paths connecting source and receiver in a complex 3-D model.

It should also be mentioned that during this search procedure, no dynamic parameters (i.e., wavefront curvature, amplitude, etc.) are calculated. Such calculations are carried out only for the resulting ray paths. These rays are traced through the medium once more, and the necessary integrations are performed in order to determine the parameters wanted.

A simple example is shown in Fig. VI.8.2. Fig. VI.8.2a shows a 3-D model, consisting of 5 interfaces. The seismic velocities in each layer are generally varying continuously with space coordinates. Fig. VI.8.2b shows a vertical cross section through the model along the line A-B in Fig. VI.8.2a, together with normal incidence rays for this line projected into the cross section. Because of the 3-D nature of the problem the ray paths will generally not intersect the interfaces in this cross section. Fig. VI.8.2c shows the corresponding zero offset seismic section. Note that each amplitude has been scaled proportional to the travel time, in order to compensate for the large dynamic range of the various arrivals.

H. Gjøystdal

J.E. Reinhardsen

References

Cerveny, V. & F. Hron, 1980: The ray series method and dynamic ray tracing system for three dimensional inhomogeneous media. Bull. Seism. Soc. Am., 70, 47-77.

Gjøystdal, H., 1978A: A general computer algorithm for calculating zero-value contours of a bivariate scalar function, with special application to seismic ray-tracing in complex 3-dimensional models. Tech. Rep. No. 4/80, NTNF/NORSAR, Kjeller, Norway.

Gjøystdal, H., 1978B: Computation of seismic ray paths øbetween given source and receiver line in a complex 3-D model. Tech. Rep. No. 3/80, NTNF/NORSAR, Kjeller, Norway.

Gjøystdal, H., 1979: Ray tracing in complex 3-D geological models: Presented at the 49th Annual International SEG Meeting, November 5, in New Orleans.

Gjøystdal, H. & B. Ursin, 1981: Inversion of reflection times in three dimensions, Geophysics, 46, 972-983.

Gjøystdal, H., J.E. Reinhardsen & B. Ursin, 1981: Travel time and wavefront curvature calculations in inhomogeneous layered media with curved interfaces, NORSAR Tech. Rep. No. 2/81, NTNF/NORSAR, Kjeller.

Hubral, P. & T. Krey, 1980: Interval velocities from seismic reflection time measurements. Society of Exploration Geophysicists, Tulsa, Oklahoma. Larner, K.L. (ed.).

Reinhardsen, J.E., 1981: Dynamic ray-tracing in complex three-dimensional geological models, NORSAR Tech. Rep. 1/81, NTNF/NORSAR, Kjeller.

'DYNAMIC' RAY-TRACING

CALCULATION OF

- RAY PATH (COORDINATES AND DIRECTION)
- TRAVEL TIME
- TRAVEL DISTANCE
- WAVEFRONT CURVATURE
- AMPLITUDE

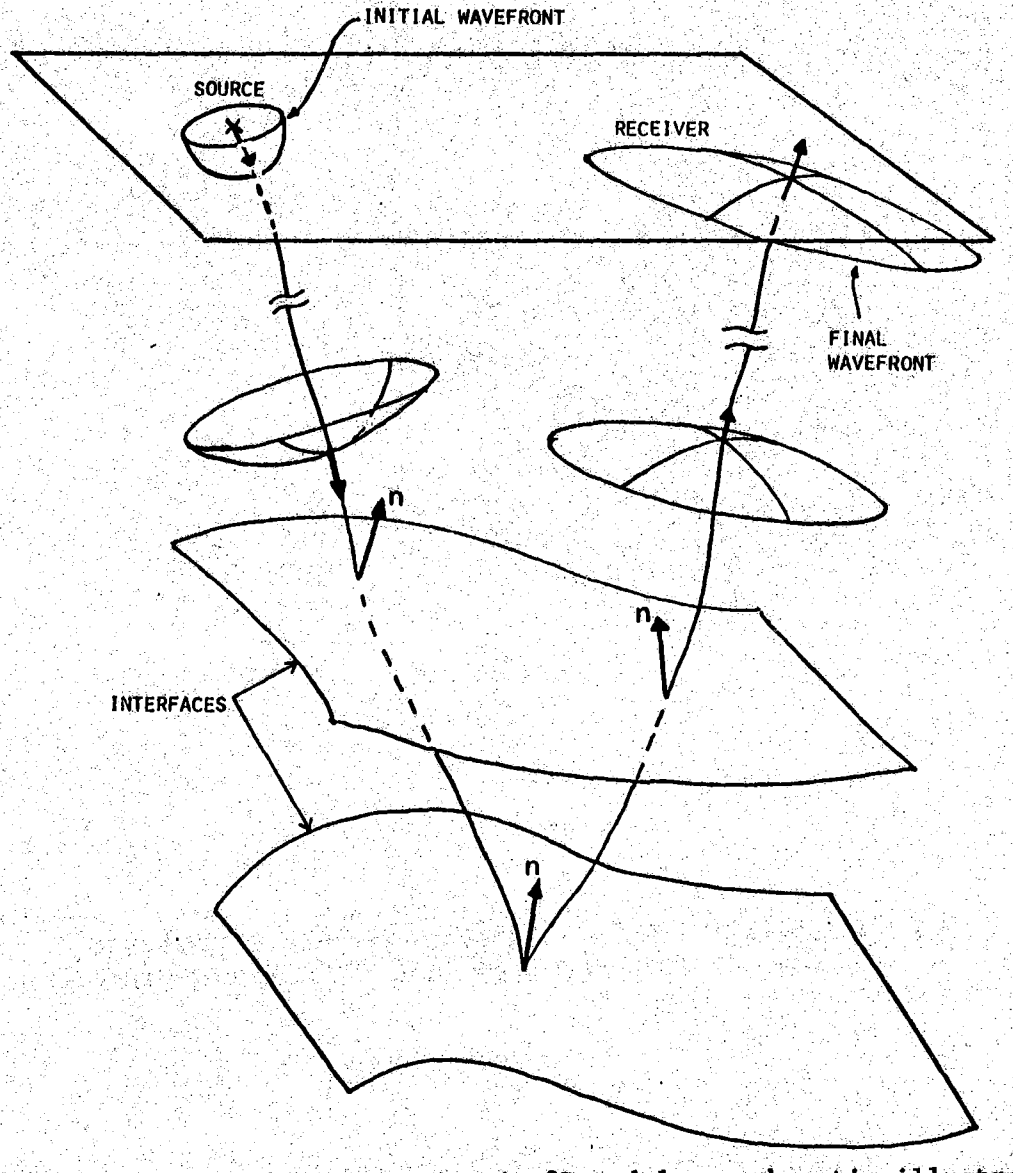

Fig. VI.8.1 Dynamic ray-tracing in 3D models - schematic illustration.

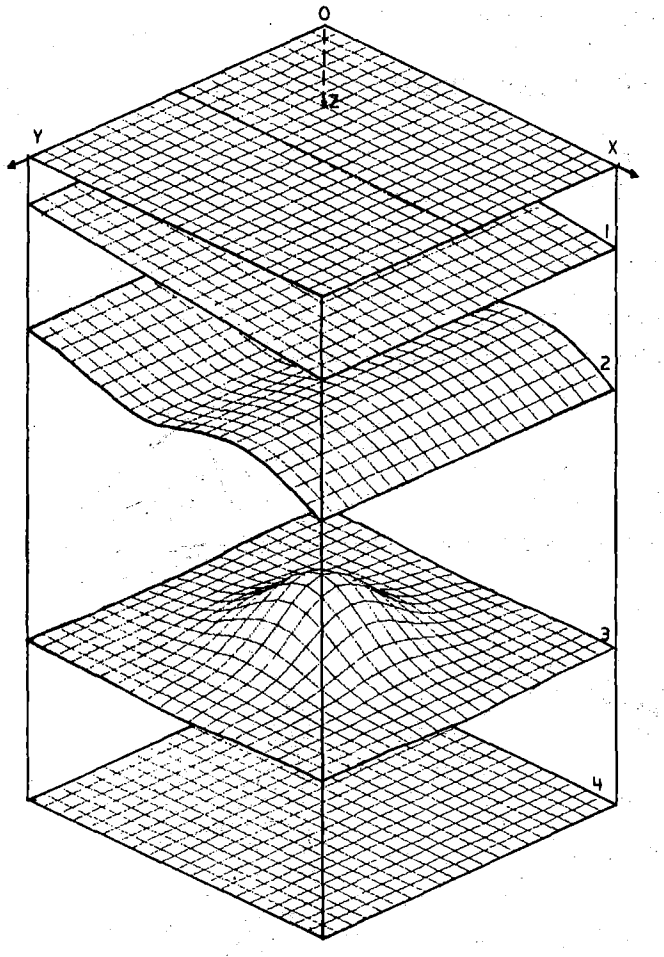

Fig. VI.8.2 (a) Three-dimensional plot of the synthetic model. Vertical scale is exaggerated. Horizon extension is 10 x 10 km; vertical extension is 4 km.

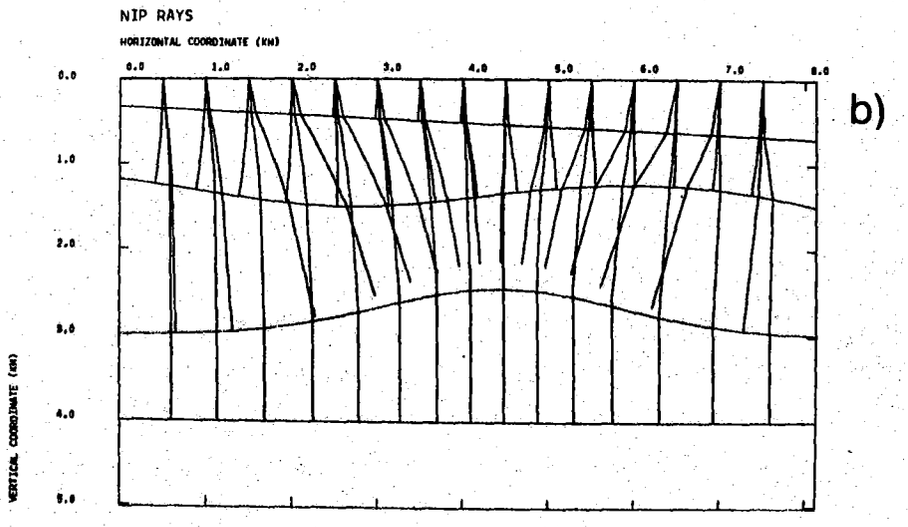

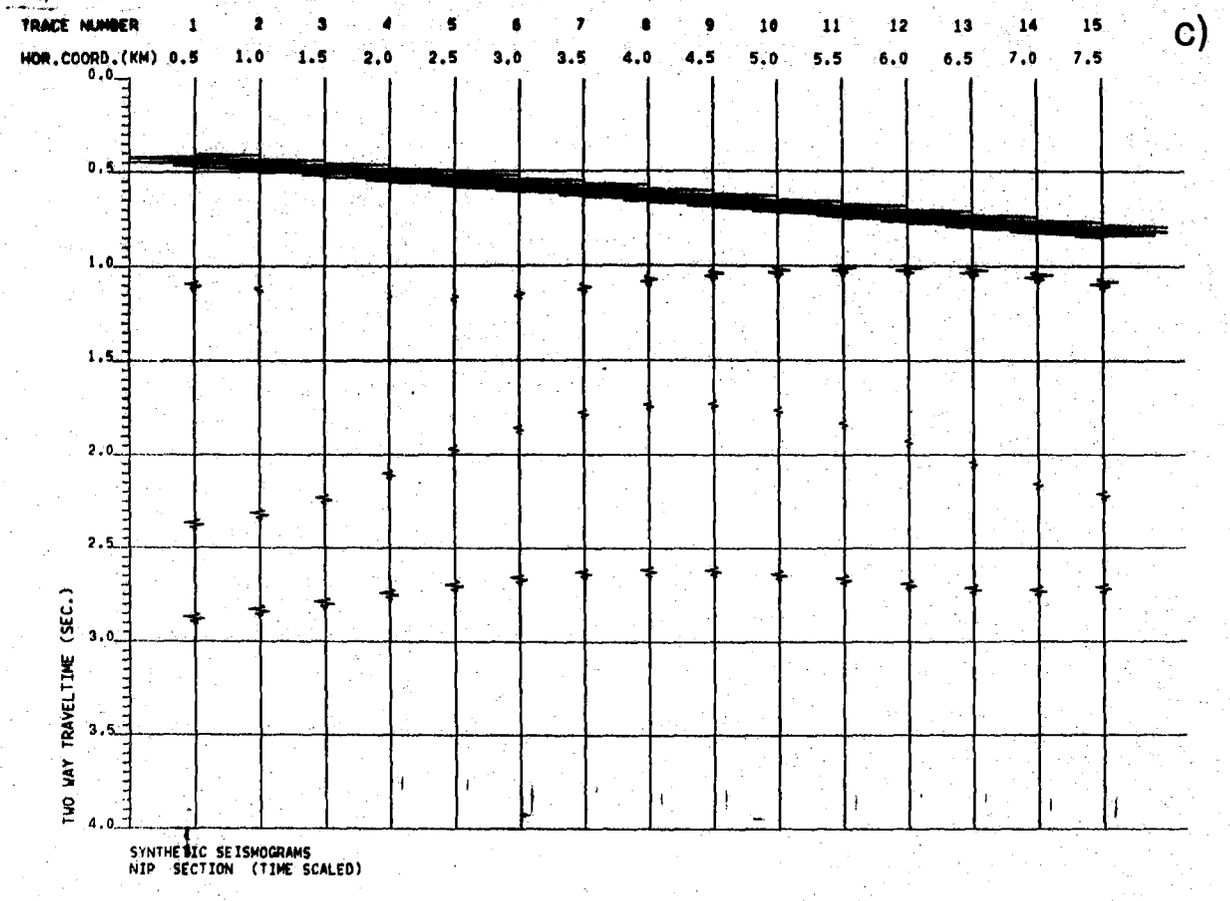

Fig. VI.82 (b) Vertical cross section of the model along the shot/receiver line. Horizontal coordinate 0.5 km is at position (2.,2.).

(c) Synthetic seismograms for a general 3-D model with nonlinear velocities. Horizontal coordinates along shot/receiver line.

VI.9 High resolution group velocity analysis AR-method

McCowan (1978) introduces a new high resolution method for measurement of group velocities of seismic surface waves. McCowan's method is based on the instantaneous frequency estimator of Griffiths (1975) which was designed to estimate the frequency content of digital signals with a narrow band and rapidly time varying spectrum. Griffiths and Prieto-Diaz (1977) used this new method, called the adaptive autoregressive (AR) method of data modelling, on seismic data and demonstrated that when conventional methods provide a poor resolution, a high resolution is still achievable by this technique.

The adaptive AR method is most useful for analysis of compact waveforms recorded at regional distances from a seismic source. It will be used for obtaining group velocities in the Middle East using data from the Seismic Research Observatories (SRO) in this region. In this report the AR method is briefly reviewed and a test case on synthetic data presented.

The basic problem is to find group arrival times on a seismogram generated by a near distance seismic source. The group arrival time at a frequency ω_o is the time of maximum energy at frequencies in the vicinity of ω_o, and is found by spectral estimations.

Denote a set of N equally spaced data points in the time series by

$$x(k),\ k = 0,1,2,\ldots,N-1$$

In the traditional methods (see for example Dziewonski and Hales, 1972), a window (say a Gaussian one) is defined appropriately, convolved with data at regular intervals and each time the amplitude spectrum is calculated by a Fourier transform. The result of this process is then contour plotted and the group arrival times picked from the contours.

In the adaptive AR method, the window (or filter) depends on past values of the signal and is continuously updated as new values become available. The updatation is performed by a simple algorithm after Widrow and Hoff (1960) which is defined as follows:

$$a_\ell(k+1) = a_\ell(k)+\mu\varepsilon(k)\chi(k-\ell) \tag{1}$$

in which the value of the filter coefficient at time (k+1), i.e., $a_\ell(k+1)$, is found from the previous filter and data values. The adaptive step size μ is a parameter which controls the convergence of the scheme and is related to the filter length L and filter learning constant α by:

$$\mu = \frac{\alpha}{L\sigma_\chi^2} \tag{2}$$

where σ_χ^2 is the input power level. The time constant of convergence for the algorithm is given by:

$$\tau = \frac{-1}{\ell n(1-\alpha/L)} \tag{3}$$

$\varepsilon(k)$ in (1) is the filter output at time k and is defined by

$$\varepsilon(k) = \chi(k)- \sum_{\ell=1}^{L} a_\ell(k)\chi(k-\ell) \tag{4}$$

and finally the spectral estimation giving the group arrival time is

$$S(\omega,k) = \left|1- \sum_{\ell=1}^{L} a_\ell(k)e^{-j\omega\ell}\right|^{-2} \tag{5}$$

(see Griffiths and Prieto-Diaz, 1977; McCowan, 1978).

It follows from (3) that the filter constants L and α determine the convergence of the algorithm. The convergence of the adaptive AR method is discussed by Griffiths (1975), Griffiths and Prieto-Diaz (1977), and McCowan (1978) where they suggest that values of between (10-20) and (0.1-2.0) should be selected for L and α respectively.

In summary, the filter parameters L and α must be selected appropriately, filter coefficients at discrete times k_1, k_2,...,k_n calculated using (1) and (4). The spectral estimates are then calculated using (5), contour plotted and group arrival times picked from the contours. If the instrument response is removed from the data prior to filtering, the contours can be calibrated to give the group velocities directly.

The adaptive AR method is capable of tracking instantaneous frequencies (Griffith, 1975). This very important feature can be demonstrated by applying the method to a pure sine wave. Take 100 samples from a 0.05 Hz sine wave (sampled at a rate of one sample per second), and define filter parameters as follows:

Filter length: $L = 12$

Filter learning constant: $\alpha = 0.20$

By using (3) the adaptive time constant will be

$$\tau = \frac{-1}{\ell n(1-\alpha/L)} = 59.50 \text{ seconds.}$$

The filter output calculated from (4) is plotted in Fig. VI.9.1a. As expected, the filter output tends to zero at times greater than the adaptive time constant (59.5 seconds), i.e., in this case the present values of the sine wave can be predicted from its past values without any error. The adaptive AR spectral estimates calculated at three different times (20, 60 and 90 seconds) are shown in Fig. VI.9.1b-1d. In Fig. VI.9.1b, the calculation is performed at a time before the adaptive time constant, and there is no spectral peak at 0.05 Hz. In Fig. VI.9.1c, at a time corresponding to a full time constant, a side lobe is still present though its amplitude is more than 12 dB below the main 0.05 Hz signal amplitude. In Fig. VI.9.1d, at a time greater than the full time constant, the side lobes fall more than 40 dB below the main signal level and thus the main signal is easily identified.

In conclusion the adapative AR method is shown to work as expected on synthetic data. The next step is to select seismic events at regional distances from SRO stations and apply this method to find group velocities for many profiles in the Middle East.

I. Asudeh

References

Dziewonski, A.M. & A.L. Hales, 1972: Numerical analysis of dispersed seismic waves. Methods of Computational Physics, Vol. 11, Seismology: Surface Waves and Earth Oscillations (Ed. B.A. Bolt), Academic Press, New York.

Griffiths, L.J., 1975: Rapid measurements of digital instantaneous frequency. IEEE Trans. Acoust. Speech Signal Process., 23, 207-222.

Griffiths, L.J. & R. Prieto-Diaz, 1977: Spectral analysis of natural seismic events using autoregressive techniques. IEEE Trans. Geoscience Electronics, Vol. GE15, No.1.

McCowan, D.W., 1978: High resolution group velocity analysis. Geoexploration, 16, 97-109.

Widrow, B. & M.E. Hoff, 1960: Adaptive switching circuits, IRE WESCON Convention Record, pt. 4, 96-104.

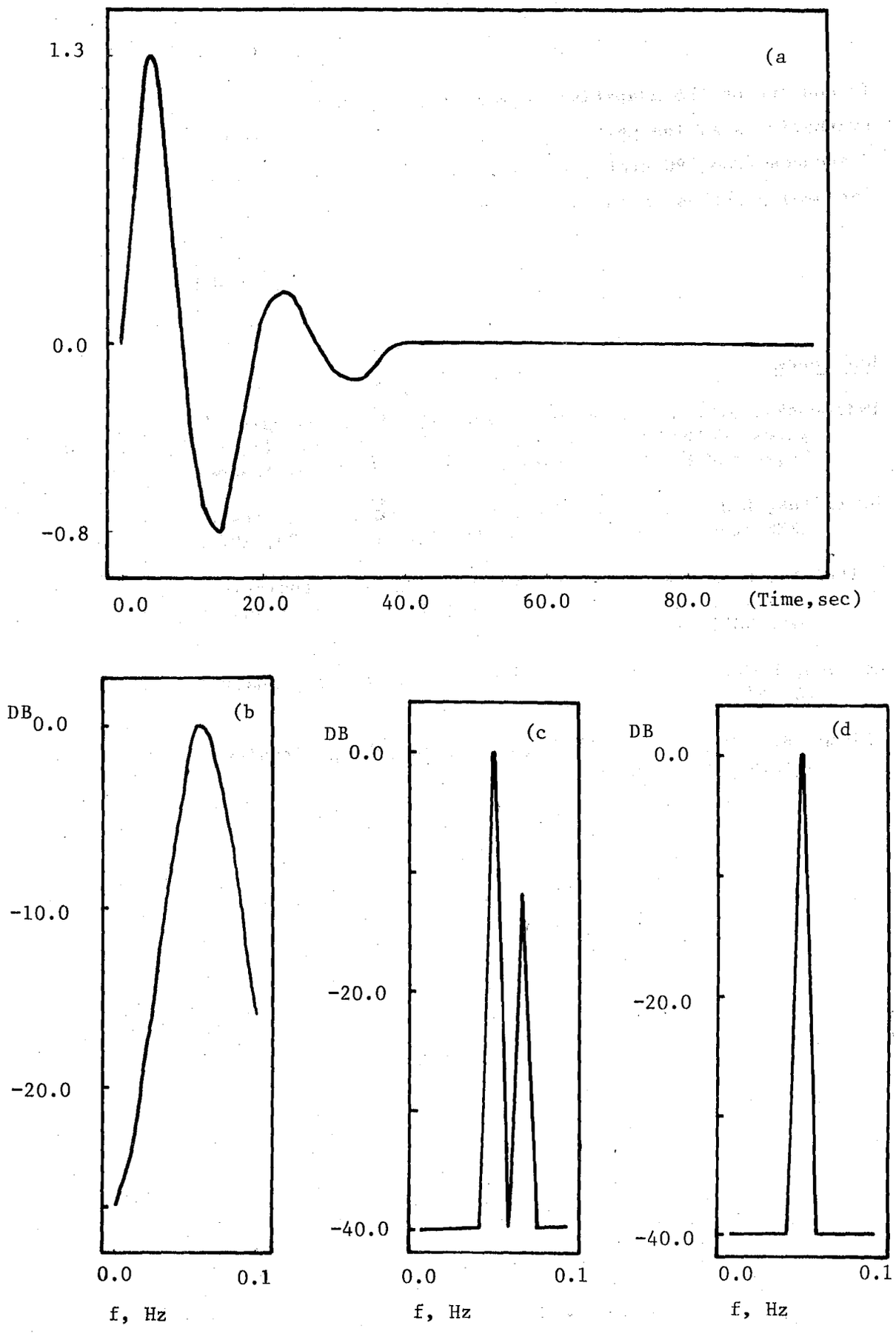

Fig. VI.9.1 Filter output tends to zero at times greater than the adaptive time constant (59.5 sec) (a). Adaptive spectral estimates are calculated at 20 sec (b), 60 sec (c), and 90 sec (d). See text.